

Quaternion-Based Dictionary Learning and Saturation-Value Total Variation Regularization for Color Image Restoration

Chaoyan Huang¹, Michael K. Ng¹, Tingting Wu¹, and Tieyong Zeng^{1,2}

Abstract—Color image restoration is a critical task in imaging sciences. Most variational methods regard the color image as a Euclidean vector or the direct combination of three monochrome images and completely ignore the inherent color structures within channels. To better describe the relationship of color channels, we represent the color image as the so-called pure quaternion matrix. Note that the celebrated dictionary learning method has attracted considerable attention for image recovery in the past decade. Following this idea, we propose a novel quaternion-based color image recovery method. This model combines the advantages of dictionary learning and the total variation method for color image restoration. The new strategy used in the proposed model manages to handle the color image restoration problem in the quaternion space. Moreover, the new proposed model can be easily solved by the classical alternating direction method of multipliers (ADMM) algorithm. Numerical results demonstrate clearly that the performance of our proposed dictionary learning method is better than some state-of-the-art color image dictionary learning and total variation methods in terms of some criteria and visual quality.

Index Terms—Dictionary learning, image restoration, pure quaternion, total variation.

I. INTRODUCTION

COLOR image restoration aims to recover a clean image from the degraded observation. In the processing of generating, transmission, and storage, the color image will be unavoidably degraded by noise and blur. As images are essential

Manuscript received April 14, 2021; revised July 13, 2021; accepted August 18, 2021. This work was supported in part by the National Key R&D Program of China under Grant 2021YFE0203700, in part by NSFC/RGC N_CUHK 415/19, RGC 14300219, 14302920, and 14301121, in part by the CUHK Direct grant for Research under Grants 4053405 and 4053460, in part by the Graduate Student Scientific Research Innovation Project of Jiangsu Province, 2020, under Grant KYCX20_0788, in part by HKRGC GRF under Grants 12300218, 12300519, 17201020, and 17300021, in part by the Natural Science Foundation of China under Grants 61971234 and 11501301, in part by the 1311 Talent Plan of NUPT, the QingLan Project for Colleges and Universities of Jiangsu Province. The associate editor coordinating the review of this manuscript and approving it for publication was Dr. Jiale (Jerry) Shen. (*Corresponding author: Tingting Wu.*)

Chaoyan Huang and Tingting Wu are with the School of Science, Nanjing University of Posts and Telecommunications, Nanjing 210003, China (e-mail: 1019081805@njupt.edu.cn; wutt@njupt.edu.cn).

Michael K. Ng is with the Department of Mathematics, The University of Hong Kong, Hong Kong (e-mail: mng@maths.hku.hk).

Tieyong Zeng is with the Department of Mathematics, The Chinese University of Hong Kong Shatin, Hong Kong (e-mail: zeng@math.cuhk.edu.hk).

Color versions of one or more figures in this article are available at <https://doi.org/10.1109/TMM.2021.3107162>.

Digital Object Identifier 10.1109/TMM.2021.3107162

in various fields such as biomedical imaging, microscopy, astronomical imaging, and multimedia processing, it is critical to restoring the sharp image from the degraded observation.

The color image processing is the extension of gray image restoration. Since color image restoration is a typical ill-posed problem, recovering the degraded image is rather challenging. In the literature, there are many excellent methods for gray image restoration. Rudin, Osher, and Fatemi [1] proposed the total variation (TV)-based method to handle the image denoising problem. Later, the TV-based model was extended by many researchers to tackle the image restoration problem, such as [2], [3]. In [4], the reliable image recovery results were generated by the dictionary learning (DL)-based method. Zeng *et al.* [5] applied the DL-based method for image denoising and yielded competitive results. The DL-based method, first introduced by Olshausen and Field [6] and continued by Elad *et al.* [7]–[9], has been applied to various tasks of image processing, such as image restoration [10], [11], image inpainting [12], [13], image recognition [14], [15], image compression [16], image classification [17], and object detection [18]. Recently, the machine learning-based method has received significant attention in image processing and has good results in image restoration. For example, Jin *et al.* [19] proposed a flexible deep convolutional neural networks (CNN) framework for image restoration. Mou *et al.* [20] restored the image with the collaborative attention network (COLA-Net). In [21], Popyan, Romano, and Elad built a nice connection between CNN and DL, which provided a new interpretation of CNN. Moreover, [22] also gave the theoretical guarantees for convolutional sparse coding. However, the integration of the DL-based method with the most recent advanced tools in image processing is still an open question.

As an important branch of image processing, DL aims at searching for a suitable dictionary where the trained data has sparse representation [23]–[26]. By minimizing the reconstruction error of the training data, the dictionary learning method can take full advantage of the sample information [27], [28]. By giving the following assumption: an image patch $\mathbf{u}_0 \in \mathbb{R}^m$ is approximately sparse under some dictionary $\mathbf{D} \in \mathbb{R}^{m \times k}$; the linear measurement $\mathbf{g}_0 = \mathbf{u}_0 + \mathbf{b}_0$ where \mathbf{b}_0 is the noise following some statistical distributions; estimating the original image patch \mathbf{u}_0 as $\mathbf{u}_0 \approx \mathbf{D}\mathbf{a}$. Then we can get \mathbf{u}_0 by solving

$$\min_{\mathbf{a}} \|\mathbf{a}\|_0, \text{s.t. } \|\mathbf{g}_0 - \mathbf{D}\mathbf{a}\|_2^2 \leq \epsilon, \quad (1)$$

73 where $\|\cdot\|_0$ denotes the ℓ_0 -norm which counts the number
 74 of non-zero elements; $\|\cdot\|_2$ represents the ℓ_2 norm, i.e.,
 75 $\|x\|_2 = \sqrt{\sum_{t=1}^l x_t^2}$ with $x = \{x_1, x_2, \dots, x_l\}$; \mathbf{a} represents the sparse coefficient vector; and $\epsilon \geq 0$ is a parameter with respect
 76 to the noise level. Once we have obtained the solution \mathbf{a} of (1),
 77 with the given dictionary \mathbf{D} , the original image patch \mathbf{u}_0 can be
 78 estimated by $\mathbf{u}_0 = \mathbf{D}\mathbf{a}$.

79 The choice of the dictionary \mathbf{D} has a significant influence
 80 on the performance of the image restoration. The dictionary \mathbf{D}
 81 can be either given or learned from observed images [29], [30].
 82 For the predetermined dictionary, such as curvelets, wavelets,
 83 and discrete cosine transforms (DCT), their computational per-
 84 formances are always faster than the learned ones. However,
 85 the predetermined dictionary is not adapted to the degraded
 86 images [4]. A trained dictionary containing the prior informa-
 87 tion can better fit the images and significantly improve recovery
 88 quality [31], [32]. Among the learned dictionaries, Ma, Yu, and
 89 Zeng [33] learned the dictionary from the corresponding de-
 90 graded image and led to competitive performance in impulse
 91 noise removal. Chen *et al.* [34] learned a compact dictionary
 92 from original contaminated samples for face recognition. In [35],
 93 the authors applied a set of image patches to train a dictionary for
 94 spectral computed tomography (CT) material decomposition.
 95 In [36], the dictionary is trained using image patches for image
 96 denoising under mixed noise. The methods above have good re-
 97 sults in their tasks. However, the dictionary can contain more
 98 prior information. Inspired by the deep learning-based method,
 99 we train the dictionary by using a set of color images.

100 Considering the color information of an image is indispens-
 101 able, and color images have wide applications in our lives. Many
 102 researchers turned to tackle color image restoration. However,
 103 most of them simply apply the techniques of the gray image to
 104 color image restoration. The dictionary learning model can well
 105 handle the gray image in [7] but generate color distribution when
 106 denoising the color image in [9]. Therefore, simply applying the
 107 gray image-based method to the color image seems not suitable.
 108 Pei and Cheng [37] claimed that there are inner-relationships be-
 109 tween the red, green, and blue (RGB) channels of color images.
 110 They represented the color image with a quaternion matrix and
 111 had better results than those used in the gray image. Recently,
 112 many works paid a lot of attention to quaternion representation.
 113 Li, Zhou, and Zhang [38] used the quaternion non-local total
 114 variation regularizer for color image denoising. Their results
 115 are better than the real-valued non-local total variation-based
 116 methods. In [39] and [40], the authors extended the low-rank
 117 matrix approximation into the quaternion domain and achieved
 118 better color image denoising results than the real-valued low
 119 rank-based methods. Xu *et al.* [41] applied the DL with quater-
 120 nion for color image denoising, inpainting, and super-resolution.
 121 They achieved good results by representing color images with
 122 the quaternion matrix. A quaternion has three imaginary parts
 123 and one real part. We consider that representing a color image
 124 with three imaginary parts is better than simply regarding the
 125 color image as a union of three independent channels.

126 Although the dictionary method achieves good results, there
 127 is still room for improvement, i.e., they cannot preserve image
 128 edges well [33]. Moreover, the simple patch-based approach will

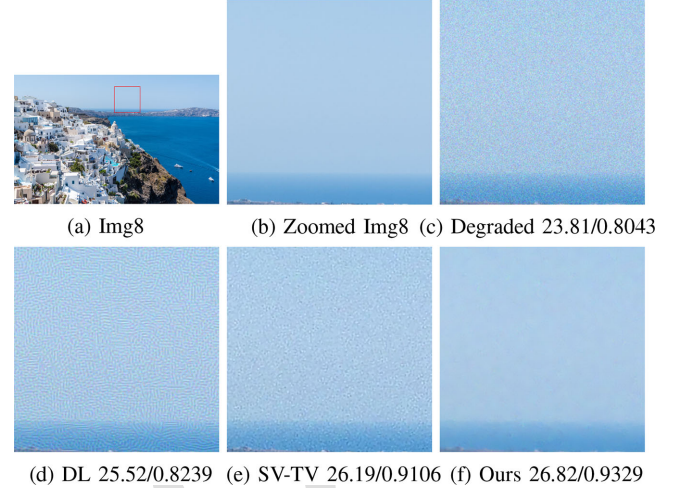


Fig. 1. The comparison of different restoration methods with visual results and PSNR/SSIM values. (a) Original image; (b) The zoomed part of Img8; (c) The zoomed part of the degraded image with Gaussian blur (15,1) and Gaussian noise level $\sigma = 12.75$; The zoomed part of images reconstructed by: (d) the dictionary learning method; (e) the SV-TV method; (f) our method.

introduce artifacts in the deblurring problem [42], [43]. Since the TV regularizer has attractive properties, i.e., convex and better sharp edge preservation [44]–[46], the TV- ℓ_1 model has been widely applied to image deblurring and denoising tasks [47], [48]. Recently, Jia, Ng, and Wang [49] proposed a TV model in HSV color space, named SV-TV, which can remove blur and noise effectively. Their study offers some important insights into our research. A brief review of the SV-TV regularizer is given in Section II.B.

In this paper, we propose a new color image restoration method with quaternion-based dictionary learning and SV-TV regularizers. As aforementioned, dictionary learning with quaternion representation can better preserve the inherent structure of the color image. Moreover, the total variation regularizer in HSV color space has better performance. Many excellent approaches have considered color image restoration with the TV-based method, non-local means-based method, or the DL-based method. However, the combination of both TV and quaternion-based DL has not been addressed in color image restoration. Moreover, due to the complexity, the quaternion-based techniques have rarely been applied in color image restoration. In this paper, we first apply the quaternion-based dictionary learning method with the SV-TV regularizer to deblur and denoise an image simultaneously. Inspired by the machine learning-based method, we train the dictionary with a large dataset. The trained dictionary can be seen as a prior. Furthermore, we do not need to train the dictionary corresponding to the input image, which saves the restoration time dramatically compared with those dictionary learning-based methods. Notably, the proposed combination model can be regarded as a general and flexible framework. Indeed, whenever necessary, one can also adopt other advanced regularizers or blocks to generate better results. In this paper, we focus on image restoration by combining dictionary learning and SV-TV regularizers for efficiency. Fig. 1 shows the comparison of different restoration methods. It is clear that the DL-based method generates great artifacts in Fig. 1(d). For the

SV-TV method, we find that some noises remained in Fig. 1(e). Our approach combines these two regularizers for color image restoration and generates a great result in Fig. 1(f). Hence, the image that we recovered has the highest numerical result and visual quality.

Indeed, the sparse representation prior is pretty good at recovering the local features in the image, and the TV term helps stabilize the restored results. Combining pure quaternion-based DL and TV regularizers, we propose a new color image restoration method. The main contributions of our method are as follows:

- Unlike the traditional color image processing, which regards the color image as the vector or the combination of monochrome images and completely ignores the inherent color structures, we represent a color image with the pure quaternion. Both denoising and deblurring are conducted to recover a color image. Due to the special calculation rules, the inner relationship among the multiple channels can be well preserved.
- We propose a new image restoration method combining quaternion-based DL and SV-TV regularizers to recover the degraded color images and achieve more competitive color image restoration results than existing methods.
- For the numerical implementation, we train a dictionary with a large dataset and then fix the trained dictionary. Based on this strategy, there is no need to train a new corresponding dictionary for each image. Meanwhile, our pre-learned dictionary can also fit the degraded images in the processing of image restoration.

Additionally, the proposed method can be used in many real applications, including multimedia computing [50], image restoration [51], [52], video enhancement [53].

The paper is organized as follows. Section II reviews the basic concept of the quaternion, the SV-TV regularization, and the classical alternating direction method of multipliers (ADMM) algorithm. The proposed method is displayed in Section III, and experimental results are in Section IV. Finally, the conclusions follow in Section V.

II. QUATERNION AND SV-TV REGULARIZATION

A. Quaternion

The quaternion matrix is proven to be a better representation for color image restoration than the real-valued matrix [54]. The quaternion was first introduced by Hamilton [55]. Assume that \mathbb{H} is a quaternion space, let $\mathbf{u}(x, y) \in \mathbb{H}$ be a quaternion, then

$$\mathbf{u}(x, y) = u_0(x, y) + u_1(x, y)\mathbf{i} + u_2(x, y)\mathbf{j} + u_3(x, y)\mathbf{k},$$

where $u_0(x, y) \in \mathbb{R}$ is the real part, $u_1(x, y)$, $u_2(x, y)$, $u_3(x, y) \in \mathbb{R}$ are the imaginary parts, and $\mathbf{i}, \mathbf{j}, \mathbf{k}$ are three fundamental quaternion units satisfying the following quaternion rules

$$\mathbf{i}^2 = \mathbf{j}^2 = \mathbf{k}^2 = \mathbf{ijk} = -1,$$

$$\mathbf{ij} = -\mathbf{ji} = \mathbf{k}, \mathbf{jk} = -\mathbf{kj} = \mathbf{i}, \mathbf{ki} = -\mathbf{ik} = \mathbf{j}.$$

Similar to complex space, if the real part $u_0(x, y) = 0$, then $\mathbf{u}(x, y)$ is called a pure quaternion. As the color image has three



Fig. 2. Color image with quaternion representation.

channels (R, G, B), we can represent a color image with the imaginary parts of the quaternion, i.e., denoting the color image as the pure quaternion

$$\mathbf{u}(x, y) = u_r(x, y)\mathbf{i} + u_g(x, y)\mathbf{j} + u_b(x, y)\mathbf{k},$$

here (x, y) refers to the pixel location of a color image \mathbf{u} , and $u_r(x, y)$, $u_g(x, y)$, $u_b(x, y)$ are the RGB channels, respectively. Fig. 2 shows how the quaternion represents the color image.

B. SV-TV Regularization

Rudin, Osher, and Fatemi first proposed the TV regularization [1] for gray image restoration, which can preserve the edge of images. The TV term can suppress artifacts generated by the patch-based methods [56]. Given an observed image \mathbf{g} , the TV model can be written as

$$\mathbf{u} = \arg \min_{\mathbf{u}} \eta \|\nabla \mathbf{u}\|_1 + \frac{1}{2} \|\mathbf{g} - \mathbf{H} * \mathbf{u}\|_2^2, \quad (2)$$

where \mathbf{u} is the latent image, \mathbf{H} is a given blur operator, $*$ is the convolutional operation, η is the positive parameter that balance the different terms, $\frac{1}{2} \|\mathbf{g} - \mathbf{H} * \mathbf{u}\|_2^2$ is the fidelity term,

$$\|\nabla \mathbf{u}\|_1 = \sum_{i=1}^m \sum_{j=1}^n \sqrt{(\mathbf{d}_x \mathbf{u})_{ij}^2 + (\mathbf{d}_y \mathbf{u})_{ij}^2}$$

is the TV regularization term, here two discrete differential operators are introduced as

$$\begin{cases} (\mathbf{d}_x \mathbf{u})_{ij} = \mathbf{u}(i, j) - \mathbf{u}(i-1, j), \\ (\mathbf{d}_y \mathbf{u})_{ij} = \mathbf{u}(i, j) - \mathbf{u}(i, j-1). \end{cases}$$

The SV-TV regularization is introduced by Jia *et al.* [49], which is the extension of TV regularization. The SV-TV can be expressed as

$$\min_{\mathbf{u}} \eta \text{SV-TV}(\mathbf{u}) + \frac{1}{2} \|\mathbf{g} - \mathbf{H} * \mathbf{u}\|_2^2, \quad (3)$$

where

$$\begin{aligned} \text{SV-TV}(\mathbf{u}) = & \sum_{i=1}^m \sum_{j=1}^n \left(\sqrt{|(\mathbf{d}_x \mathbf{u})_{ij}|_s^2 + |(\mathbf{d}_y \mathbf{u})_{ij}|_s^2} \right. \\ & \left. + \alpha \sqrt{|(\mathbf{d}_x \mathbf{u})_{ij}|_v^2 + |(\mathbf{d}_y \mathbf{u})_{ij}|_v^2} \right), \end{aligned} \quad (4)$$

here $\alpha > 0$ is the weight of the value component. The norm $|\cdot|_s$ and $|\cdot|_v$ are defined as

$$\begin{aligned} |(\mathbf{d}_x \mathbf{u})_{ij}|_s &= \frac{1}{3} \|\mathbf{C}(\mathbf{d}_x \mathbf{u})_{ij}^T\|_2, \\ |(\mathbf{d}_y \mathbf{u})_{ij}|_s &= \frac{1}{3} \|\mathbf{C}(\mathbf{d}_y \mathbf{u})_{ij}^T\|_2, \\ |(\mathbf{d}_x \mathbf{u})_{ij}|_v &= \frac{1}{\sqrt{3}} |(\mathbf{d}_x u_r)_{ij} + (\mathbf{d}_x u_g)_{ij} + (\mathbf{d}_x u_b)_{ij}|, \\ |(\mathbf{d}_y \mathbf{u})_{ij}|_v &= \frac{1}{\sqrt{3}} |(\mathbf{d}_y u_r)_{ij} + (\mathbf{d}_y u_g)_{ij} + (\mathbf{d}_y u_b)_{ij}|, \end{aligned} \quad (5)$$

where $\mathbf{C} = \begin{bmatrix} 2 & -1 & -1 \\ -1 & 2 & -1 \\ -1 & -1 & 2 \end{bmatrix}$. We refer the interested readers

to [49] for a more comprehensive review of the SV-TV regularizer. Our proposed model applies the SV-TV regularizer to denote the piecewise-constant image part, such that the artifacts accompanied with the patch-based method can be removed.

C. ADMM Algorithm

The alternating direction method of multipliers (ADMM) algorithm [57]–[59] aims to solve the problem with the following form

$$\min_x f(x) + h(Bx). \quad (6)$$

Here, $f(x)$ and $h(Bx)$ are two convex functions, B is a constant. Let $z = Bx$, the augmented Lagrangian of (6) is

$$L_\delta(x, z; y) = f(x) + h(z) + \langle y, Bx - z \rangle + \frac{\delta}{2} \|Bx - z\|_2^2,$$

where y is called the Lagrange multiplier and δ is the penalty parameter. The ADMM algorithm consists of the iterations as follows

$$\begin{aligned} x &= \arg \min_x f(x) + \langle y, Bx - z \rangle + \frac{\delta}{2} \|Bx - z\|_2^2, \\ z &= \arg \min_z h(z) + \langle y, Bx - z \rangle + \frac{\delta}{2} \|Bx - z\|_2^2, \\ y &= y + \delta(Bx - z). \end{aligned}$$

By alternating updates x and z subproblems and the Lagrange multiplier y , the optimal solution x with guaranteed convergence is obtained. One can have a detailed comprehending in [60], the Matlab examples and related works can be found in https://stanford.edu/boyd/papers/admm_distr_stats.html.

III. OUR METHOD

In this section, we first give the proposed method. Then provide the strategy of training the dictionary. The numerical algorithm of the proposed model is also presented. Finally, we give the computation complexity of the proposed algorithm.

TABLE I
NOTATIONS USED THROUGH THE PAPER

\mathbf{u}_0	the image patch
\mathbf{D}	the dictionary
\mathbf{b}_0	the Gaussian noise
\mathbf{a}	the sparse coefficient vector
\mathbf{a}_{ij}	the sparse coefficient for the patch located at (i, j)
\mathbf{A}	the set of \mathbf{a}_{ij}
ϵ	the parameter with respect to noise level
\mathbb{H} and \mathbb{R}	the quaternion space and the real space
$w_0(x, y)$	the real part of a quaternion function
$w_t(x, y)$	the imaginary part of a quaternion function, $t = 1, 2, 3$
$u_k(x, y)$	the RGB part of an image, $k = r, g, b$
$\mathbf{i}, \mathbf{j}, \mathbf{k}$	the fundamental quaternion units
$\mathbf{u}(x, y)$	the quaternion function
\mathbf{u}	the latent image
\mathbf{g}	the observed image
η, α, λ	the positive parameter that balance the different term
$\ \cdot\ _t$	the ℓ_t -norm, $t = 0, 1, 2$
∇	the gradient operator
$\ \nabla \mathbf{u}\ _1$	the TV term
$*$	the convolutional operation
\mathbf{H}	the blur operator
$(\mathbf{d}_x \mathbf{u})_{ij}$	discrete differential operator of x orientation in location (i, j)
$(\mathbf{d}_y \mathbf{u})_{ij}$	discrete differential operator of y orientation in location (i, j)
$ \cdot _s$ and $ \cdot _v$	the s -norm and the v -norm
\mathbf{P}, \mathbf{P}_0 and \mathbf{P}_0^T	orthogonal matrices and the conjugate transpose of \mathbf{P}_0
\mathbf{J}	the singular value matrix of \mathbf{C}
\mathbf{q}	the linear transformation of \mathbf{u}
\mathbf{q}_t	three components of \mathbf{q} , $t = 1, 2, 3$
ρ_{ij}	the positive weight for patch at location (i, j)
\mathcal{R}_{ij}	the extract operator in location (i, j)
$\tilde{\mathbf{H}}, \tilde{\mathbf{g}}, \tilde{\mathbf{D}}, \tilde{\mathbf{a}}_{ij}$	the corresponding linear transformation with \mathbf{P}
$\mathbf{w}_t^x, \mathbf{w}_t^y$	auxiliary variables in ADMM algorithm, $t = 1, 2, 3$
τ_t^x, τ_t^y	Lagrangian multipliers $t = 1, 2, 3$
β	the penalty parameter

A. Proposed Scheme

Given an observed image \mathbf{g} and the blur operator \mathbf{H} , the proposed model is given as

$$\begin{aligned} \min_{\mathbf{a}_{ij}, \mathbf{u}} \lambda \|\mathbf{g} - \mathbf{H} \star \mathbf{u}\|_2^2 + \eta \text{SV-TV}(\mathbf{u}) \\ + \sum_{i,j} \rho_{ij} \|\mathbf{a}_{ij}\|_0 + \sum_{i,j} \|\mathbf{D} \mathbf{a}_{ij} - \mathcal{R}_{ij} \mathbf{u}\|_2^2, \end{aligned} \quad (7)$$

where λ and η are two positive parameters, \mathbf{u} is the ideal latent image. The second term $\text{SV-TV}(\mathbf{u})$ is the regularizer proposed in the HSV color space. The last two terms are the dictionary learning model, where ρ_{ij} is the positive patch-specific weight, the binary matrix \mathcal{R}_{ij} extracts the local patch in an image, \mathbf{D} is a pre-learned dictionary, and \mathbf{a}_{ij} is the sparse coefficient vector. The set of \mathbf{a}_{ij} is denoted as \mathbf{A} . Fig. 3 summarized our approach with the pre-learned dictionary. Table I gives a list of notations used in this paper.

B. Learning the Dictionary With K-QSVD Algorithm

The last two terms in (7) are corresponding to the above-mentioned sparsity assumption (1) (for some dictionary). In the dictionary learning part, the training images are collected from the training set of the DIV2K Dataset [61]. We download 800 training images and crop them into small patches of size 8×8 . We then learned a dictionary from these image patches with the

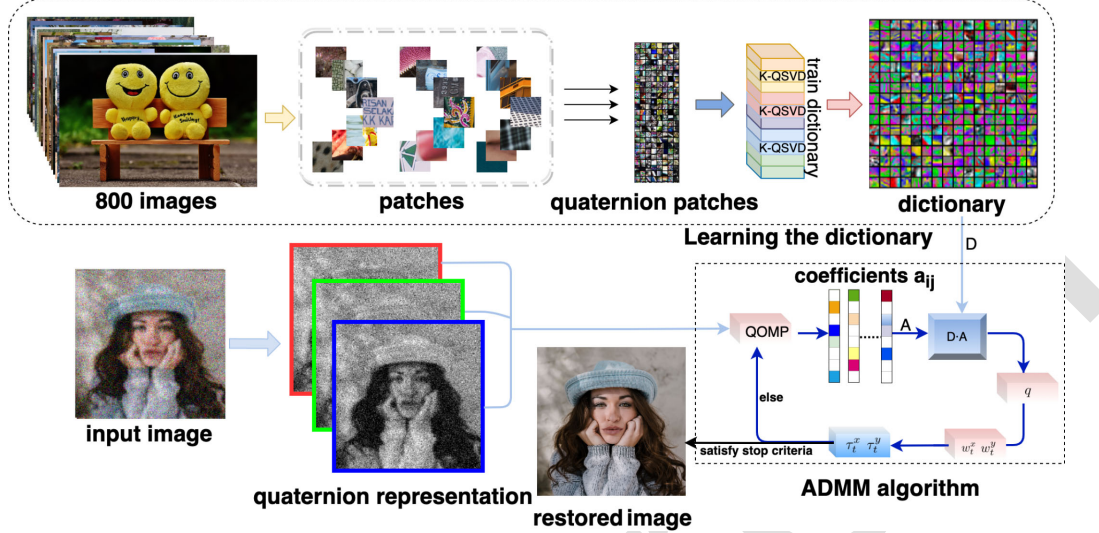


Fig. 3. The flowchart of our method.

generalized k-means clustering for quaternion singular value decomposition (K-QSVD) algorithm¹ [41]. The learned dictionary D is with the size of $64 \times 256 \times 4$. It takes 291.75 seconds in Matlab R2020a under macOS Catalina 10.15.4 with a 1.40 GHz CPU and 8 GB memory. The number of nonzero entries in \mathbf{a}_{ij} is called the sparsity level of \mathbf{a}_{ij} . In this paper, the sparsity level is set to be 5, which is the default value in the K-QSVD algorithm. After the dictionary is learned, we fix it for all image restoration. Fig. 3 contains the processing of dictionary training.

C. Numerical Algorithm of the Proposed Model (7)

To better solve the proposed model, we first perform a linear transformation. Since the component of SV-TV ((4)) satisfies the (5). Given the orthogonal decomposition of \mathbf{C} , i.e., $\mathbf{C} = \mathbf{P}_0^T \mathbf{J} \mathbf{P}_0$, where \mathbf{P}_0 is the orthogonal matrix and

$$\mathbf{J} = \begin{bmatrix} 3 & 0 & 0 \\ 0 & 3 & 0 \\ 0 & 0 & 0 \end{bmatrix}, \mathbf{P}_0 = \begin{bmatrix} \frac{1}{\sqrt{2}} & \frac{-1}{\sqrt{2}} & 0 \\ \frac{1}{\sqrt{6}} & \frac{1}{\sqrt{6}} & \frac{-2}{\sqrt{6}} \\ \frac{1}{\sqrt{3}} & \frac{1}{\sqrt{3}} & \frac{1}{\sqrt{3}} \end{bmatrix}, \quad (8)$$

following (8), by doing the linear transformation of \mathbf{u} , we have

$$\mathbf{q} = \begin{bmatrix} \mathbf{q}_1(x, y) \\ \mathbf{q}_2(x, y) \\ \mathbf{q}_3(x, y) \end{bmatrix} = \mathbf{P}\mathbf{u} = \mathbf{P} \begin{bmatrix} u_r(x, y) \\ u_g(x, y) \\ u_b(x, y) \end{bmatrix}, \quad (9)$$

here

$$\mathbf{P} = \begin{bmatrix} \frac{1}{\sqrt{2}}\mathbf{I} & \frac{-1}{\sqrt{2}}\mathbf{I} & \mathbf{0} \\ \frac{1}{\sqrt{6}}\mathbf{I} & \frac{1}{\sqrt{6}}\mathbf{I} & \frac{-2}{\sqrt{6}}\mathbf{I} \\ \frac{1}{\sqrt{3}}\mathbf{I} & \frac{1}{\sqrt{3}}\mathbf{I} & \frac{1}{\sqrt{3}}\mathbf{I} \end{bmatrix},$$

and \mathbf{I} is the identity matrix. With the fixed \mathbf{P} , by doing the linear transformation, we set $\tilde{\mathbf{H}} = \mathbf{P}\mathbf{H}\mathbf{P}^T$, $\tilde{\mathbf{g}} = \mathbf{P}\mathbf{g}$, $\tilde{\mathbf{D}} = \mathbf{P}\mathbf{D}$,

¹The code of the K-QSVD algorithm can be found in [Online]. Available: <https://lichengunc.github.io/>.

$\tilde{\mathbf{a}}_{ij} = \mathbf{a}_{ij}$. The objective function (7) is reformulated as

$$\min_{\tilde{\mathbf{a}}_{ij}, \mathbf{q}} \lambda \|\tilde{\mathbf{H}} * \mathbf{q} - \tilde{\mathbf{g}}\|_2^2 + \eta \text{SV-TV}(\mathbf{q}) + \sum_{i,j} \rho_{ij} \|\tilde{\mathbf{a}}_{ij}\|_0 + \sum_{i,j} \|\tilde{\mathbf{D}}\tilde{\mathbf{a}}_{ij} - \mathcal{R}_{ij}\mathbf{q}\|_2^2, \quad (10)$$

where

$$\begin{aligned} \text{SV-TV}(\mathbf{q}) = & \sum_{i=1}^m \sum_{j=1}^n (\alpha \sqrt{(\mathbf{d}_x \mathbf{q}_3)_{ij}^2 + (\mathbf{d}_y \mathbf{q}_3)_{ij}^2} \\ & + \sqrt{(\mathbf{d}_x \mathbf{q}_1)_{ij}^2 + (\mathbf{d}_x \mathbf{q}_2)_{ij}^2 + (\mathbf{d}_y \mathbf{q}_1)_{ij}^2 + (\mathbf{d}_y \mathbf{q}_2)_{ij}^2}). \end{aligned} \quad (11)$$

Following previous works [41], [49], we can establish the optimization scheme based on the ADMM approach [57]–[59]. According to II-C, by introducing auxiliary variables $\mathbf{w}_t^x, \mathbf{w}_t^y$, Lagrangian multipliers τ_t^x and τ_t^y ($t = 1, 2, 3$), and a penalty parameter $\beta > 0$, we have the augmented Lagrangian of the proposed model as follows

$$\begin{aligned} L_\beta(\tilde{\mathbf{a}}_{ij}, \mathbf{q}, \mathbf{w}_t^x, \mathbf{w}_t^y; \tau_t^x, \tau_t^y) &= \sum_{i=1}^m \sum_{j=1}^n \left(\lambda \|\tilde{\mathbf{H}} * \mathbf{q} - \tilde{\mathbf{g}}\|_2^2 + \rho_{ij} \|\tilde{\mathbf{a}}_{ij}\|_0 + \|\tilde{\mathbf{D}}\tilde{\mathbf{a}}_{ij} - \mathcal{R}_{ij}\mathbf{q}\|_2^2 \right. \\ &+ \eta \left(\sqrt{|(\mathbf{w}_1^x)_{ij}|^2 + |(\mathbf{w}_2^x)_{ij}|^2 + |(\mathbf{w}_1^y)_{ij}|^2 + |(\mathbf{w}_2^y)_{ij}|^2} \right. \\ &+ \alpha \sqrt{|(\mathbf{w}_3^x)_{ij}|^2 + |(\mathbf{w}_3^y)_{ij}|^2} \left. \right) + \sum_{t=1}^3 (\langle \tau_t^x, (\mathbf{w}_t^x - \mathbf{d}_x \mathbf{q}_t)_{ij} \rangle \\ &+ \langle \tau_t^y, (\mathbf{w}_t^y - \mathbf{d}_y \mathbf{q}_t)_{ij} \rangle + \frac{\beta}{2} \|(\mathbf{w}_t^x - \mathbf{d}_x \mathbf{q}_t)_{ij}\|_2^2 \\ &\left. \left. + \frac{\beta}{2} \|(\mathbf{w}_t^y - \mathbf{d}_y \mathbf{q}_t)_{ij}\|_2^2 \right) \right). \end{aligned} \quad (12)$$

Then the solution is derived by alternatively solving the following three subproblems.

309

- $\tilde{\mathbf{a}}_{ij}$ -subproblem

$$\min_{\tilde{\mathbf{a}}_{ij}} \sum_{i=1}^m \sum_{j=1}^n (\rho_{ij} \|\tilde{\mathbf{a}}_{ij}\|_0 + \|\tilde{\mathbf{D}}\tilde{\mathbf{a}}_{ij} - \mathcal{R}_{ij}\mathbf{q}\|_2^2), \quad (13)$$

310 following (1), given an observed image \mathbf{g} , the corresponding coefficient vectors \mathbf{a}_{ij} can be obtained. We apply the quaternion orthogonal matching pursuit (QOMP) algorithm² to get \mathbf{a}_{ij} .

- q-subproblem

$$\begin{aligned} \min_{\mathbf{q}} \lambda \|\tilde{\mathbf{H}} \star \mathbf{q} - \tilde{\mathbf{g}}\|_2^2 + \sum_{i=1}^m \sum_{j=1}^n & \|\tilde{\mathbf{D}}\tilde{\mathbf{a}}_{ij} - \mathcal{R}_{ij}\mathbf{q}\|_2^2 \\ & + \sum_{t=1}^3 (\langle \tau_t^x, (\mathbf{w}_t^x - \mathbf{d}_x \mathbf{q}_t)_{ij} \rangle + \langle \tau_t^y, (\mathbf{w}_t^y - \mathbf{d}_y \mathbf{q}_t)_{ij} \rangle) \\ & + \frac{\beta}{2} \|(\mathbf{w}_t^x - \mathbf{d}_x \mathbf{q}_t)_{ij}\|_2^2 + \frac{\beta}{2} \|(\mathbf{w}_t^y - \mathbf{d}_y \mathbf{q}_t)_{ij}\|_2^2, \end{aligned} \quad (14)$$

315 then the q-subproblem has a close form solution

$$\mathbf{q} = \frac{2\lambda \tilde{\mathbf{H}}^T \tilde{\mathbf{g}} + 2 \sum_{i,j} \mathcal{R}_{ij}^T \tilde{\mathbf{D}}\tilde{\mathbf{a}}_{ij} + \Xi}{2\lambda \tilde{\mathbf{H}}^T \tilde{\mathbf{H}} + 2 \sum_{i,j} \mathcal{R}_{ij}^T \mathcal{R}_{ij} + \beta(\mathbf{d}_x^T \mathbf{d}_x + \mathbf{d}_y^T \mathbf{d}_y)}, \quad (15)$$

316 where $\Xi = \sum_{t=1}^3 (\tau_t^x \mathbf{d}_x + \tau_t^y \mathbf{d}_y + \beta(\mathbf{d}_x^T \mathbf{w}_t^x + \mathbf{d}_y^T \mathbf{w}_t^y))$.
317 • \mathbf{w}_t^x and \mathbf{w}_t^y -subproblem ($t = 1, 2, 3$)
318 It is a typical problem that can be solved by the soft shrinkage algorithm [62]. According to the soft shrinkage algorithm, we have the solution of \mathbf{w}_t^x and \mathbf{w}_t^y as follows
320

$$\begin{aligned} \mathbf{w}_1^x &= \max(s_1 - \frac{\eta}{\beta}, 0) \frac{\mathbf{d}_1^x - \mathbf{w}_1^x/\beta}{s_1}, \\ \mathbf{w}_1^y &= \max(s_1 - \frac{\eta}{\beta}, 0) \frac{\mathbf{d}_1^y - \mathbf{w}_1^y/\beta}{s_1}, \\ \mathbf{w}_2^x &= \max(s_1 - \frac{\eta}{\beta}, 0) \frac{\mathbf{d}_2^x - \mathbf{w}_2^x/\beta}{s_1}, \\ \mathbf{w}_2^y &= \max(s_1 - \frac{\eta}{\beta}, 0) \frac{\mathbf{d}_2^y - \mathbf{w}_2^y/\beta}{s_1}, \\ \mathbf{w}_3^x &= \max(s_2 - \frac{\eta\alpha}{\beta}, 0) \frac{\mathbf{d}_3^x - \mathbf{w}_3^x/\beta}{s_2}, \\ \mathbf{w}_3^y &= \max(s_2 - \frac{\eta\alpha}{\beta}, 0) \frac{\mathbf{d}_3^y - \mathbf{w}_3^y/\beta}{s_2}, \end{aligned} \quad (16)$$

321 where

$$\begin{aligned} s_1 &= \sqrt{\sum_{t=1}^2 (\mathbf{d}_x - \frac{\mathbf{w}_t^x}{\beta})^2 + (\mathbf{d}_y - \frac{\mathbf{w}_t^y}{\beta})^2}, \\ s_2 &= \sqrt{(\mathbf{d}_x - \frac{\mathbf{w}_3^x}{\beta})^2 + (\mathbf{d}_y - \frac{\mathbf{w}_3^y}{\beta})^2}. \end{aligned} \quad (17)$$

- 322 • τ_t^x and τ_t^y -subproblem ($t = 1, 2, 3$)

²The code of the QOMP algorithm can be found in [Online]. Available: <https://lichengunc.github.io/>.

Algorithm 1: Our algorithm for image Restoration.

Initialization Represent color image with quaternion matrix. Given the pre-learned dictionary \mathbf{D} and the orthogonal matrix \mathbf{P} . Set $\mathbf{u} = \mathbf{g}$. Choose parameters $\lambda, \eta, \alpha, \beta$. Set the maximum iteration T .
for iteration=1 to T **do**
 Update $\tilde{\mathbf{a}}_{ij}$ with (13);
 Update \mathbf{q} using (15);
 Update \mathbf{w}_t^x and \mathbf{w}_t^y using (16);
 Update τ_t^x and τ_t^y using (18);
 $T = T + 1$.
end for
return $\mathbf{u} = \mathbf{P}^{-1}\mathbf{q}$.



Fig. 4. Ground-truth images.

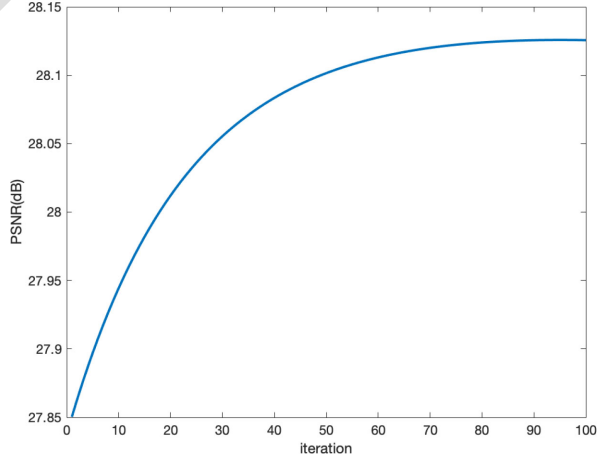


Fig. 5. PSNR values of results recovered from Img6 with 'degraded=fspecial('Gaussian',15,1)+noise' by the proposed method.

323 The Lagrange multipliers are updated as follows.

$$\tau_t^x = \tau_t^x + \beta(\mathbf{w}_t^x - \mathbf{d}_x), \quad \tau_t^y = \tau_t^y + \beta(\mathbf{w}_t^y - \mathbf{d}_y). \quad (18)$$

324 By iterating \mathbf{a}_{ij} , \mathbf{q} , \mathbf{w}_t^x , and \mathbf{w}_t^y -subproblems and Lagrange
325 multipliers τ_t^x and τ_t^y ($t = 1, 2, 3$) with Eqs. (13)-(17), the
326 optimal solution \mathbf{q} is obtained. Since \mathbf{P} is an orthogonal matrix,
327 we can get the solution \mathbf{u} from (9). Our optimization scheme is
328 summarized in Algorithm 1.

D. Computation Complexity

329 The computation complexity also plays an important role in
330 determining the final performance of the proposed framework.
331 Suppose that we have M samples with dimension $m \times n \times 3$
332

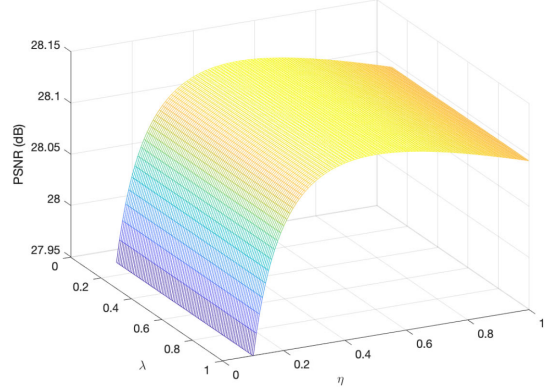
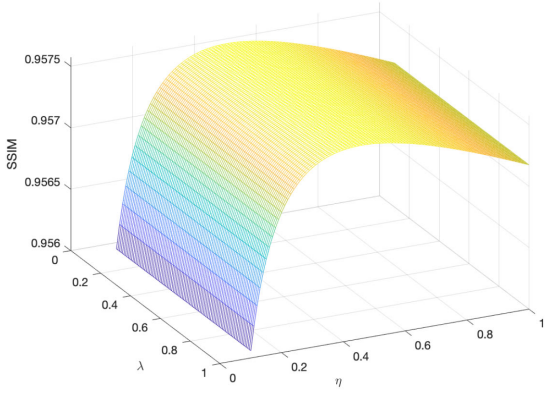
(a) PSNR values along with η and λ .(b) SSIM values along with η and λ .

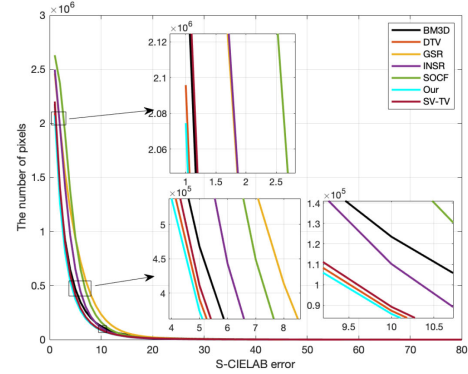
Fig. 6. Restoration results of Img6 with different parameters.

333 corresponding to color patches. The dictionary size is $m \times n \times 3 \times K$, where K is the number of atoms. The sparsity constraint
 334 is $3L$ for the sparse code of each color channel. As a result,
 335 according to [41], the complexity of the QOMP algorithm is
 336 $\mathcal{O}(LM(\frac{14 \times m \times n}{3})^3)$, the complexity of the K-QSVD algorithm
 337 is $\mathcal{O}(LM(\frac{13 \times m \times n}{3})^3)$. The iteration of the proposed method in
 338 Algorithm 1 is T . In every iteration, we need to update \tilde{a}_{ij} with
 339 the QOMP algorithm. Overall, the complexity of our method as
 340 a whole is $\mathcal{O}(TLM(\frac{14 \times m \times n}{3})^3)$.
 341

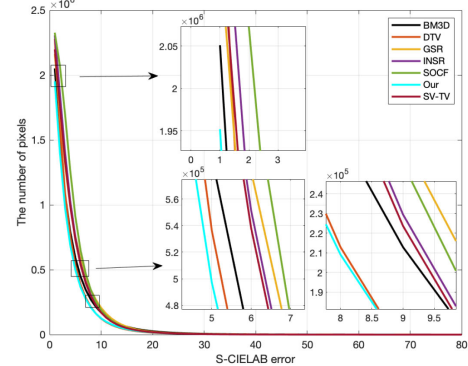
IV. EXPERIMENTAL RESULTS

342 To demonstrate the effectiveness of our quaternion-based dic-
 343 tionary learning and total variation method, we present the nu-
 344 matical and visual results in this section. We compare the pro-
 345 posed method with TV-based models (DTV [63], SV-TV [49]),
 346 DL-based methods (GSR [64], INSR [65]), sharpening opera-
 347 tor combined with framelet model (SOCF [66]), and the classic
 348 image processing method (BM3D [67]) for image restoration³.
 349

³The code of SV-TV [49] and SOCF [66] were provided by the corresponding authors; the code of DTV [63] was downloaded from [Online]. Available: <https://sites.google.com/site/thunsukeono/publications>; the code of GSR [64] was downloaded from [Online]. Available: <https://github.com/jianzhangcs/GSR>; the code of INSR [65] was downloaded from [Online]. Available: https://github.com/WanglifuCV/INSR_Deblur-SR; the code of BM3D [67] was downloaded from [Online]. Available: <https://webpages.tuni.fi/foi/GCF-BM3D/>.



(a) Results with ‘degraded=fspecial(‘gaussian’,15,1)+noise’.



(b) Results with ‘degraded=fspecial(‘gaussian’,15,1.5)+noise’.

Fig. 7. The average S-CIELAB errors between the ground-truth images and the restored results.

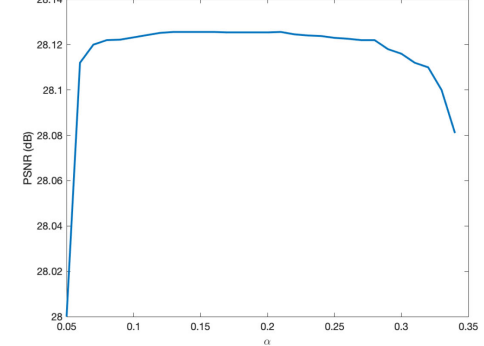
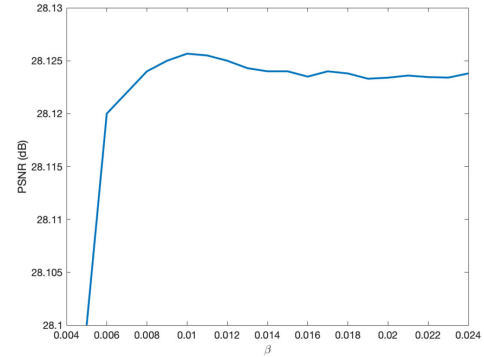
(a) PSNR values along with parameter α .(b) PSNR values along with parameter β .

Fig. 8. Parameters analysis. PSNR results of Img6 with ‘degraded=fspecial(‘Gaussian’,15,1)+noise’ by the proposed method.

TABLE II
PSNR AND SSIM VALUES OF COLOR IMAGE RESTORATION WITH GAUSSIAN KERNEL (15,1) AND NOISE LEVEL $\sigma = 12.75$

Images\Methods	Degraded	SOCF [66]	BM3D [67]	DTV [63]	SV-TV [49]	GSR [64]	INSR [65]	Ours
	PSNR SSIM	PSNR SSIM	PSNR SSIM	PSNR SSIM	PSNR SSIM	PSNR SSIM	PSNR SSIM	PSNR SSIM
Img1	25.70 0.8489	30.56 0.9556	32.76 0.9788	32.17 0.9480	32.24 0.9461	32.62 0.9662	31.93 0.9068	33.17 0.9826
Img2	27.37 0.8655	29.20 0.9583	35.02 0.9927	34.41 0.9519	34.39 0.9492	34.31 0.9802	34.99 0.9875	35.87 0.9929
Img3	25.54 0.7683	29.03 0.9084	30.19 0.9368	31.84 0.9492	31.23 0.9461	31.78 0.9325	31.82 0.9300	32.05 0.9357
Img4	23.54 0.6445	25.19 0.8094	25.63 0.8934	25.46 0.8996	26.12 0.8345	25.08 0.7963	25.36 0.7718	26.24 0.8996
Img5	22.96 0.7030	24.19 0.8282	24.01 0.8365	24.77 0.8790	24.87 0.8602	24.12 0.7932	24.86 0.8324	25.09 0.8872
Img6	24.38 0.7076	26.50 0.8094	26.95 0.8758	26.55 0.8519	26.62 0.8563	26.92 0.8914	27.23 0.9025	28.11 0.8932
Img7	25.05 0.6266	28.19 0.8439	28.28 0.8453	28.55 0.9100	28.78 0.9302	29.04 0.8619	29.11 0.8632	29.99 0.9193
Img8	23.81 0.8043	25.66 0.8883	25.83 0.8902	26.29 0.9243	26.19 0.9106	25.56 0.8696	25.52 0.8239	26.82 0.9329
Img9	24.71 0.7764	27.37 0.9050	27.96 0.9249	28.05 0.9363	28.33 0.8994	28.95 0.9324	28.97 0.9217	28.94 0.9370
Img10	24.57 0.7761	26.98 0.8857	27.78 0.8976	26.49 0.8820	26.67 0.9210	28.03 0.9025	28.18 0.9339	28.77 0.9551
Img11	24.52 0.6752	26.94 0.8329	27.60 0.8355	26.53 0.9111	26.84 0.9228	26.65 0.8767	26.77 0.7613	28.59 0.9030
Img12	23.87 0.7996	25.72 0.8767	26.15 0.8771	26.68 0.8914	26.64 0.8852	25.27 0.8582	25.12 0.8042	26.87 0.8915
Img13	24.22 0.6981	26.36 0.8547	26.64 0.8792	27.03 0.9044	27.00 0.8637	26.01 0.8292	25.81 0.8144	27.67 0.9052
Img14	24.14 0.6897	26.61 0.8766	27.64 0.9217	27.19 0.9200	27.60 0.8252	27.03 0.8950	27.12 0.8641	27.69 0.9192
Img15	24.93 0.5607	27.86 0.7826	28.48 0.8264	29.23 0.8576	29.22 0.8002	29.81 0.8195	29.73 0.8311	29.82 0.8537
Aver.	25.09 0.7295	27.92 0.8758	29.30 0.9036	29.10 0.9118	29.19 0.8997	29.51 0.9058	29.59 0.8892	30.29 0.9336

TABLE III
PSNR AND SSIM VALUES OF COLOR IMAGE RESTORATION WITH GAUSSIAN KERNEL (15,1.5) AND NOISE LEVEL $\sigma = 12.75$

Images\Methods	Degraded	SOCF [66]	BM3D [67]	DTV [63]	SV-TV [49]	GSR [64]	INSR [65]	Ours
	PSNR SSIM	PSNR SSIM	PSNR SSIM	PSNR SSIM	PSNR SSIM	PSNR SSIM	PSNR SSIM	PSNR SSIM
Img1	25.41 0.8445	30.59 0.9642	32.66 0.9806	31.94 0.9745	32.32 0.9725	32.64 0.9674	31.95 0.8809	32.72 0.9771
Img2	25.48 0.8824	29.93 0.9734	34.73 0.9918	33.56 0.9897	33.88 0.9809	33.85 0.8983	34.95 0.9885	
Img3	25.02 0.7428	28.87 0.9073	30.72 0.9150	29.08 0.8886	30.38 0.9145	31.00 0.9154	30.87 0.8538	31.18 0.9397
Img4	22.21 0.6002	23.78 0.8138	23.99 0.8562	24.56 0.8928	24.79 0.8559	23.87 0.7513	23.67 0.6482	24.91 0.8568
Img5	21.81 0.6549	23.09 0.8067	23.11 0.8077	23.04 0.8491	23.45 0.8428	22.56 0.7519	22.88 0.6960	23.53 0.8532
Img6	23.32 0.6621	25.60 0.8344	27.04 0.8774	26.63 0.8419	27.32 0.8812	27.31 0.8620	27.12 0.8893	27.33 0.8937
Img7	24.33 0.5859	27.20 0.8233	28.66 0.8530	28.35 0.8185	28.68 0.8348	28.80 0.8353	29.01 0.8141	29.20 0.8631
Img8	22.71 0.7632	24.59 0.8667	24.60 0.8602	25.04 0.8973	25.17 0.8983	23.77 0.8005	23.77 0.8005	25.65 0.9074
Img9	23.72 0.7449	26.17 0.8946	27.55 0.9192	27.54 0.9012	27.04 0.8773	29.81 0.8195	28.59 0.8632	29.91 0.9274
Img10	23.66 0.7433	26.03 0.8753	27.55 0.8989	27.35 0.8748	27.72 0.9025	28.00 0.8966	28.26 0.8605	28.27 0.8875
Img11	23.50 0.6214	25.64 0.7985	27.41 0.8335	26.17 0.7936	27.84 0.8426	27.88 0.8339	27.64 0.8604	27.49 0.8733
Img12	23.27 0.7763	25.32 0.8685	25.72 0.8695	25.28 0.8791	25.30 0.8794	23.61 0.7856	23.61 0.7856	26.03 0.8795
Img13	23.04 0.6549	25.11 0.8449	25.26 0.8505	24.94 0.8752	24.82 0.8708	24.16 0.7811	24.27 0.6947	25.58 0.8789
Img14	22.84 0.6603	24.77 0.8688	26.89 0.9189	28.60 0.8958	26.97 0.8522	30.03 0.8950	29.76 0.9023	30.34 0.8884
Img15	24.29 0.5248	27.29 0.7916	28.83 0.8348	28.58 0.8069	29.06 0.8198	29.81 0.8195	28.99 0.7946	29.83 0.8626
Aver.	23.64 0.6975	26.27 0.8621	27.30 0.8686	27.66 0.8944	27.71 0.8823	27.81 0.8464	27.62 0.8162	28.46 0.8983

350 The numerical quality of the restored images is measured by
351 S-CIELAB error⁴ [68], PSNR (peak signal-to-noise ratio), and
352 SSIM (structural similarity index measure) [69]. All test ex-
353 periments are conducted in MATLAB R2020a under macOS
354 Catalina 10.15.4 with a 1.40 GHz CPU and 8 GB memory.

355 A. Parameter Setting

356 The Dataset DIV2K⁵ [61] has a training set and a test set.
357 There are 800 images in the training set and 200 images in the
358 test set. We make use of images⁶ in Fig. 4 taken from the test set
359 of the DIV2K Dataset to test the proposed model for color image
360 restoration. We simulate the degraded images by convoluting
361 the original image in Fig. 4 with different Gaussian blur levels
362 (Matlab language *degraded=fspecial('Gaussian',15,1)*, and
363 *fspecial('Gaussian',15,1.5)*). Furthermore, we add the Gaussian
364 noise to model the unavoidable noise degradation in image

365 processing. For Gaussian blur (15,1), we set $\lambda = 0.5$, $\eta = 0.5$,
366 $\alpha = 0.22$, $\beta = 0.01$ for our method. For Gaussian blur (15,1.5),
367 we set $\eta = 0.4$. The parameters of other methods are the default
368 values or the corresponding values described in their articles
369 and codes. We break the ADMM iteration when the relative
370 error of the successive iterates is less than or equal to 10^{-5} for
371 all the testing methods.

372 B. Our Strategy

373 With the fixed dictionary, by updating the subproblems under
374 the framework of the ADMM algorithm, the final restoration re-
375 sult is obtained. The convergence of Img6 is given in Fig. 5 to
376 illustrate the effectiveness of the proposed model. As the itera-
377 tion goes, the PSNR (dB) value is going to stability. Due to the
378 proposed model combines different regularizers for color image
379 restoration, we display the analysis of the balance parameters η
380 and λ in a small interval in Fig. 6. In the test, we choose differ-
381 ent η and λ by trial and error to produce the best possible result.
382 The PSNR and SSIM curves become quite flat as the parameter η
383 from 0.3 to 0.8 along the η axis, which implies choosing $\eta = 0.5$
384 ensures the best result of the test Img6. We choose the parameter
385 η in the interval [0.3,0.8] for other test images. The curve along

⁴S-CIELAB code is in [Online]. Available: <http://scarlet.stanford.edu/brian/scielab/scielab.html>.

⁵[Online]. Available: <https://data.vision.ee.ethz.ch/cvl/DIV2K/>.

⁶Image size: Img1, 2, 3, 7, 10, 11, 12, 13 with 2040 × 1356; Img 4, 5 with 2040 × 1536; Img 6 with 2040 × 1200; Img 14 with 2040 × 1152; Img 8 with 2040 × 1284; Img 9 with 1356 × 2040; Img 15 with 2040 × 2040.

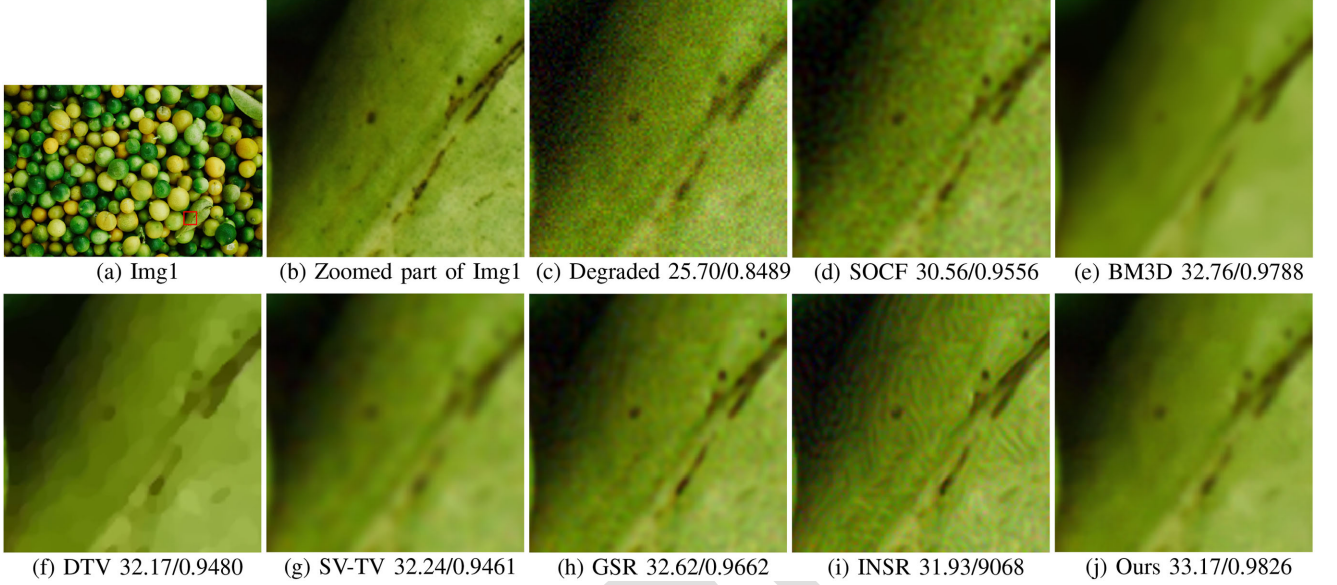


Fig. 9. Color image restoration results on Img1. (a) Original image; (b) The zoomed part of Img1; (c) Gaussian blur (15,1) and Gaussian noise level $\sigma = 12.75$; The zoomed part of restored image reconstructed by: (d) SOCF [66], (e) BM3D [67], (f) DTV [63], (g) SV-TV [49], (h) GSR [64], (i) INSR [65], and (j) Ours.

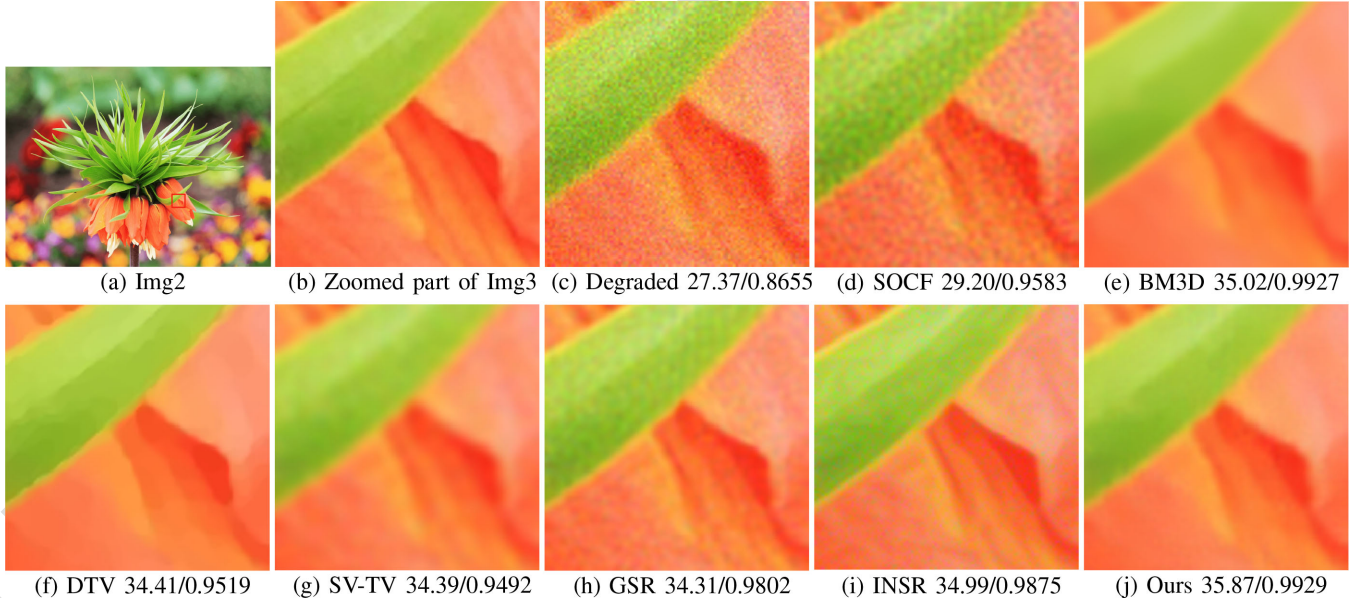


Fig. 10. Color image restoration results on Img2. (a) Original image; (b) The zoomed part of Img2; (c) Gaussian blur (15,1) and Gaussian noise level $\sigma = 12.75$; The zoomed part of restored image reconstructed by: (d) SOCF [66], (e) BM3D [67], (f) DTV [63], (g) SV-TV [49], (h) GSR [64], (i) INSR [65], and (j) Ours.

386 λ almost has a wider peak in $(0.1, 0.9]$, which gives more choices
387 of λ . Here, we find a small interval $(0.1, 0.9]$, such that the results
388 are robust to the parameter λ . The analysis of parameters α and
389 β are also conducted in Fig. 8. We set $\alpha \in [0.05, 0.34]$ with step
390 size 0.01 and $\beta \in [0.005, 0.015]$ with step size 0.001. How to
391 select the related parameters automatically is an open question.
392 We leave this as future works.

393 C. Experimental Results

394 Since the CIELAB system [70] is an important international
395 standard for measuring color reproduction errors, we test the
396 results with the S-CIELAB error indicator [68]. The S-CIELAB

397 error evaluates the error between a pair of images. For 15 images
398 in Fig. 4, we find that when the S-CIELAB error becomes 70,
399 all the error pixels number of restored images by the methods
400 we tested equate to zero. We set the error from 0 to 80 so that
401 the S-CIELAB indicator can calculate the error number of these
402 image pairs. Here error = 0 means the two images are the same.
403 As the S-CIELAB error goes, the number of error pixels decreases.
404 We plot the average S-CIELAB errors of all 15 images in Fig. 7,
405 which shows the restored image of our method has the least total
406 error pixel number. It becomes clear that the proposed method
407 outperforms other testing methods in terms of the S-CIELAB
408 color metric when the S-CIELAB error less than 10 units.



Fig. 11. Color image restoration results on Img6. (a) Original image; (b) The zoomed part of Img6; (c) Gaussian blur (15,1) and Gaussian noise level $\sigma = 12.75$; The zoomed part of restored image reconstructed by: (d) SOCF [66], (e) BM3D [67], (f) DTV [63], (g) SV-TV [49], (h) GSR [64], (i) INSR [65], and (j) Ours.

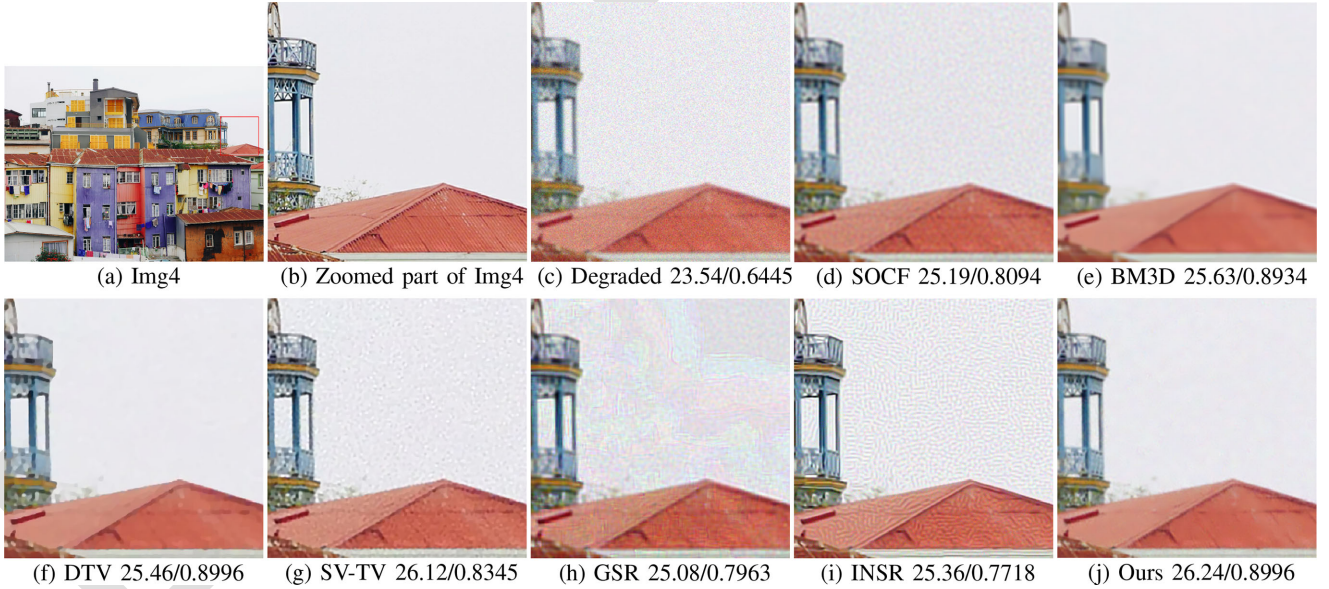


Fig. 12. Color image restoration results on Img4. (a) Original image; (b) The zoomed part of Img4; (c) Gaussian blur (15,1.5) and Gaussian noise level $\sigma = 12.75$; The zoomed part of restored image reconstructed by: (d) SOCF [66], (e) BM3D [67], (f) DTV [63], (g) SV-TV [49], (h) GSR [64], (i) INSR [65], and (j) Ours.

409 The numerical results of the SSIM and PSNR values are
 410 present in Table II and Table III. The highest PSNR and SSIM
 411 values are highlighted in bold and the second-highest ones are
 412 underlined. The average PSNR and SSIM values of all compared
 413 methods are also computed. We find that most of our results out-
 414 perform other competing methods' results in terms of the PSNR
 415 and SSIM values, which further verifies the advantages of our
 416 method. For visual quality, we display the recovered results of
 417 our experiments in Fig. 9, Fig. 10, and Fig. 11 for the blur ker-
 418 nel of standard deviation 1 and white Gaussian noise of standard

419 deviation $\sigma = 12.75$. Fig. 12, Fig. 13, and Fig. 14 show the blur
 420 kernel of standard deviation 1.5 and white Gaussian noise of
 421 standard deviation $\sigma = 12.75$. The quality of the restored images
 422 can be evaluated visually besides the values. From the visual re-
 423 sults, we know that the restored images of the SOCF method still
 424 have some color spots. The DTV method tends to smooth the
 425 textures in the restored images. The SV-TV method is good at
 426 handling image noise, while the results show that this method is
 427 not very expert in blur removal. For the classical BM3D method,
 428 the results seem to oversmooth. As for the dictionary learning

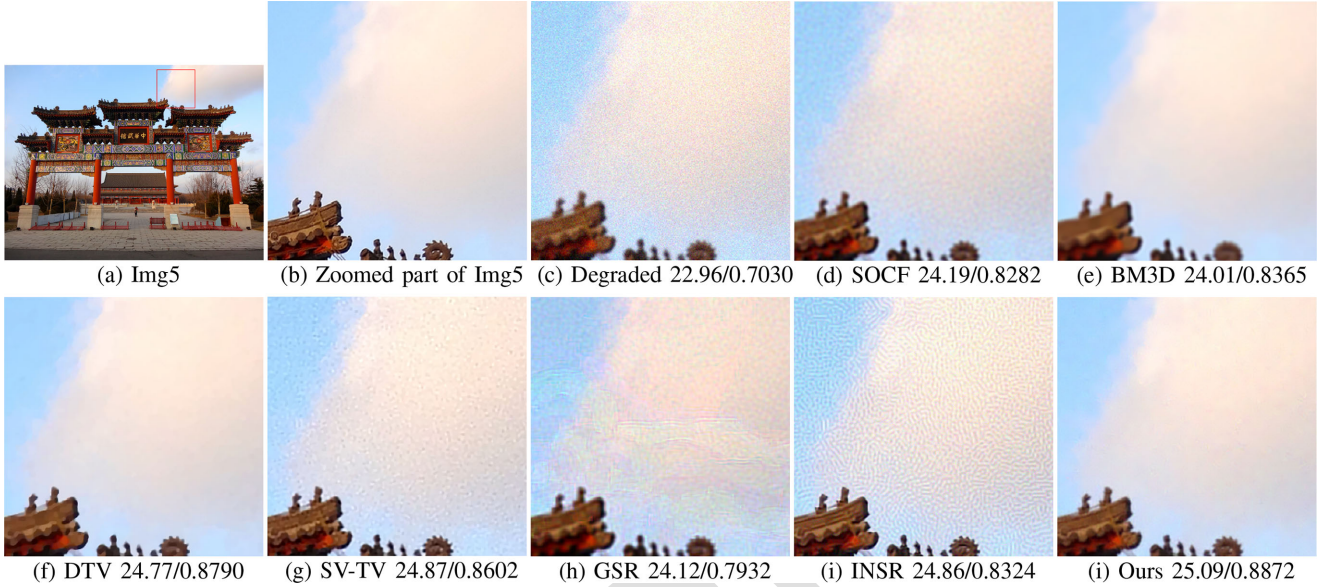


Fig. 13. Color image restoration results on Img5. (a) Original image; (b) The zoomed part of Img5; (c) Gaussian blur (15, 1.5) and Gaussian noise level $\sigma = 12.75$; The zoomed part of restored image reconstructed by: (d) SOCF [66], (e) BM3D [67], (f) DTV [63], (g) SV-TV [49], (h) GSR [64], (i) INSR [65], and (j) Ours.

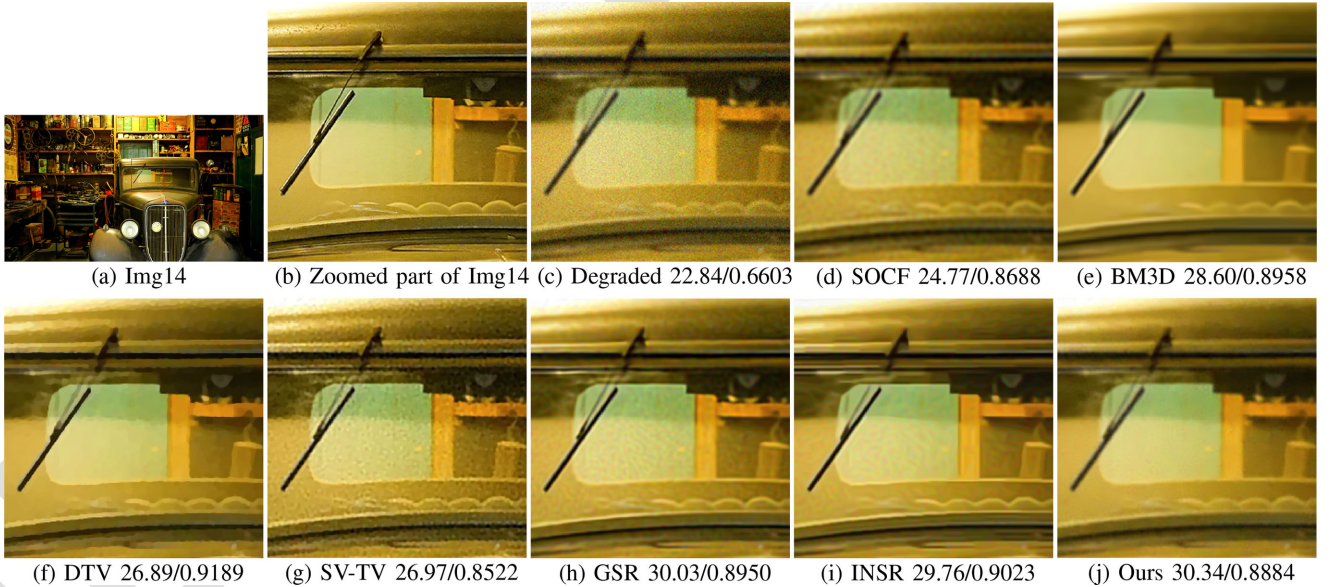


Fig. 14. Color image restoration results on Img14. (a) Original image; (b) The zoomed part of Img14; (c) Gaussian blur (15, 1.5) and Gaussian noise level $\sigma = 12.75$; The zoomed part of restored image reconstructed by: (d) SOCF [66], (e) BM3D [67], (f) DTV [63], (g) SV-TV [49], (h) GSR [64], (i) INSR [65], and (j) Ours.

429 method INSR and GSR, the artifacts can be found clearly. Our
430 method can better restore the degraded images and remove the
431 artifacts generated by the patch-based method.

432 V. CONCLUSION

433 In this paper, we propose an effective method that combines
434 pure quaternion dictionary learning and SV-TV regularizers for
435 color image recovery. For color image processing, we represent
436 the color image with the pure quaternion matrix. In this case,
437 the inner relationship of the color image can be well preserved.

438 The patch-based dictionary learning method always generates
439 some unsatisfied artifacts. We apply SV-TV to overcome these
440 artifacts. Compared with some state-of-the-art image restoration
441 methods, our model can preserve more texture details and avoid
442 the generation of artifacts. In summary, the method we proposed
443 achieves great success in numerical and visual results.

444 Since the parameters of different test images are quite differ-
445 ent, it may not be good enough to tune parameters manually.
446 Hence, how to determine the parameters automatically will be
447 our future work.

448

449 [1] L. I. Rudin, S. Osher, and E. Fatemi, "Nonlinear total variation based noise
450 removal algorithms," *Physica D: Nonlinear Phenomena*, vol. 60, no. 1-4,
451 pp. 259–268, 1992.
452 [2] L. Ma, L. Moisan, J. Yu, and T. Zeng, "A dictionary learning approach
453 for poisson image deblurring," *IEEE Trans. Med. Imag.*, vol. 32, no. 7,
454 pp. 1277–1289, Jul. 2013.
455 [3] K. Bredies, K. Kunisch, and T. Pock, "Total generalized variation," *SIAM J. Imag. Sci.*, vol. 3, pp. 492–526, 2010.
456 [4] Y. Xu and W. Yin, "A fast patch-dictionary method for whole image re-
457covery," *Inverse Problems Imag.*, vol. 10, no. 2, pp. 563–583, 2016.
458 [5] X. Zeng, W. Bian, W. Liu, J. Shen, and D. Tao, "Dictionary pair learning on
459 Grassmann manifolds for image denoising," *IEEE Trans. Image Process.*,
460 vol. 24, no. 11, pp. 4556–4569, Nov. 2015.
461 [6] B. A. Olshausen and D. J. Field, "Emergence of simple-cell receptive field
462 properties by learning a sparse code for natural images," *Nature*, vol. 381,
463 no. 6583, pp. 607–609, 1996.
464 [7] M. Aharon, M. Elad, and A. Bruckstein, "K-SVD: An algorithm for de-
465signing overcomplete dictionaries for sparse representation," *IEEE Trans. Signal
466 Process.*, vol. 54, no. 11, pp. 4311–4322, Nov. 2006.
467 [8] M. Elad and M. Aharon, "Image denoising via sparse and redundant re-
468presentations over learned dictionaries," *IEEE Trans. Image Process.*, vol. 15,
469 no. 12, pp. 3736–3745, Dec. 2006.
470 [9] J. Mairal, M. Elad, and G. Sapiro, "Sparse representation for color im-
471age restoration," *IEEE Trans. Image Process.*, vol. 17, no. 1, pp. 53–69,
472 Jan. 2008.
473 [10] E. Newman and M. E. Kilmer, "Nonnegative tensor patch dictionary ap-
474proaches for image compression and deblurring applications," *SIAM J. Imag. Sci.*,
475 vol. 13, no. 3, pp. 1084–1112, 2020.
476 [11] J. Liu and S. Osher, "Block matching local SVD operator based sparsity
477 and TV regularization for image denoising," *J. Sci. Comput.*, vol. 78, no. 1,
478 pp. 607–624, 2019.
479 [12] A. Colomer, V. Naranjo, K. Engan, and K. Skretting, "Retinal ves-
480sel inpainting using recursive least square dictionary learning algo-
481rithm," in *Proc. Int. Conf. Image Process. Theory, Tools Appl.*, 2015,
482 pp. 429–433.
483 [13] Y. Naderahmadian and S. Beheshti, "Generalized adaptive weighted re-
484cursive least squares dictionary learning for retinal vessel inpainting," in
485 *Proc. IEEE Stat. Signal Process. Workshop*, 2018, pp. 40–44.
486 [14] L. Wang, S. Wang, D. Kong, and B. Yin, "Hardness-aware dictionary
487learning: Boosting dictionary for recognition," *IEEE Trans. Multimedia*,
488 pp. 1–11, Aug. 2020, doi: [10.1109/TMM.2020.3017916](https://doi.org/10.1109/TMM.2020.3017916).
489 [15] S. Zhan, J. Wang, F. M. Yang, and Q. Fang, "Gaussian mixture sparse
490 representation for image recognition based on gabor features and dictionary
491learning," *Chin. J. Electron.*, vol. 43, no. 3, pp. 523–528, 2015.
492 [16] M. Nejati, S. Samavi, N. Karimi, S. M. R. Soroushmehr, and K. Najarian,
493 "Boosted dictionary learning for image compression," *IEEE Trans. Image
494Process.*, vol. 25, no. 10, pp. 4900–4915, Oct. 2016.
495 [17] M. Yang, L. Zhang, X. Feng, and D. Zhang, "Sparse representation based
496fisher discrimination dictionary learning for image classification," *Int. J.
497Comput. Vis.*, vol. 109, no. 3, pp. 209–232, 2014.
498 [18] X. Huang, W. Feng, and H. Ping, "Moving-object detection based on sparse
499representation and dictionary learning," *Aasri Procedia*, vol. 1, no. 3,
500 pp. 492–497, 2012.
501 [19] Z. Jin et al., "A flexible deep CNN framework for image restoration," *IEEE
502Trans. Multimedia*, vol. 22, no. 4, pp. 1055–1068, Apr. 2020.
503 [20] C. Mou, J. Zhang, X. Fan, H. Liu, and R. Wang, "COLA-Net: Collaborative
504attention network for image restoration," *IEEE Trans. Multimedia*,
505 pp. 1–11, 2021.
506 [21] V. Papyan, Y. Romano, and M. Elad, "Convolutional neural networks an-
507alyzed via convolutional sparse coding," *J. Mach. Learn. Res.*, vol. 18,
508 no. 1, pp. 2887–2938, 2017.
509 [22] V. Papyan, J. Sulam, and M. Elad, "Working locally thinking globally: The-
510oretical guarantees for convolutional sparse coding," *IEEE Trans. Signal
511Process.*, vol. 65, no. 21, pp. 5687–5701, Nov. 2017.
512 [23] Y. Zheng et al., "Multi-kernel coupled projections for domain adaptive dic-
513tionary learning," *IEEE Trans. Multimedia*, vol. 21, no. 9, pp. 2292–2304,
514 Sep. 2019.
515 [24] A. Abdi, M. Rahmati, and M. M. Ebadzadeh, "Entropy based dictionary
516learning for image classification," *Pattern Recognit.*, vol. 110, 2021, Art.
517 no. 107634.
518 [25] Y. Naderahmadian, S. Beheshti, and M. A. Tinati, "Correlation based on-
519line dictionary learning algorithm," *IEEE Trans. Signal Process.*, vol. 64,
520 no. 3, pp. 592–602, Feb. 2016.

REFERENCES

- [26] K. Skretting and K. Engan, "Recursive least squares dictionary learning algorithm," *IEEE Trans. Signal Process.*, vol. 58, no. 4, pp. 2121–2130, Apr. 2010.
[27] C. Yang, J. Shen, J. Peng, and J. Fan, "Image collection summarization via dictionary learning for sparse representation," *Pattern Recognit.*, vol. 46, pp. 948–961, 2013.
[28] R. Xu, Y. Xu, and Y. Quan, "Factorized tensor dictionary learning for visual tensor data completion," *IEEE Trans. Multimedia*, vol. 23, pp. 1225–1238, May 2020.
[29] I. Tasic and P. Frossard, "Dictionary learning," *IEEE Signal Process. Mag.*, vol. 28, no. 2, pp. 27–38, Mar. 2011.
[30] B. Bao, G. Zhu, J. Shen, and S. Yan, "Robust image analysis with sparse representation on quantized visual features," *IEEE Trans. Image Process.*, vol. 22, no. 3, pp. 860–871, Mar. 2013.
[31] J. Liu et al., "Image-set based face recognition using K-SVD dictionary learning," *Int. J. Mach. Learn. Cybern.*, vol. 10, pp. 1051–1064, 2019.
[32] J. Liu, X.-C. Tai, H. Huang, and Z. Huan, "A weighted dictionary learning model for denoising images corrupted by mixed noise," *IEEE Trans. Image Process.*, vol. 22, no. 3, pp. 1108–1120, Mar. 2013.
[33] L. Ma, J. Yu, and T. Zeng, "Sparse representation prior and total variation-based image deblurring under impulse noise," *SIAM J. Imag. Sci.*, vol. 6, no. 4, pp. 2258–2284, 2013.
[34] Z. Chen, X. Wu, H. Yin, and J. Kittler, "Noise-robust dictionary learning with slack block-diagonal structure for face recognition," *Pattern Recognit.*, vol. 100, pp. 1–38, 2020.
[35] W. Wu et al., "Dictionary learning based image-domain material decomposition for spectral CT," *Phys. Med. Biol.*, vol. 65, no. 24, pp. 1–10, 2020.
[36] H. Zhu and M. K. Ng, "Structured dictionary learning for image denoising under mixed Gaussian and impulse noise," *IEEE Trans. Image Process.*, vol. 29, pp. 6680–6693, May 2020.
[37] S. Pei and C. Cheng, "A novel block truncation coding of color images using a quaternion-moment-preserving principle," *IEEE Trans. Commun.*, vol. 45, no. 5, pp. 583–595, May 1997.
[38] X. Li, Y. Zhou, and J. Zhang, "Quaternion non-local total variation for color image denoising," in *Proc. IEEE Int. Conf. Syst., Man Cybern.*, 2019, pp. 1602–1607.
[39] Y. Chen, X. Xiao, and Y. Zhou, "Low-rank quaternion approximation for color image processing," *IEEE Trans. Image Process.*, vol. 29, pp. 1426–1439, Sep. 2019.
[40] Y. Yu, Y. Zhang, and S. Yuan, "Quaternion-based weighted nuclear norm minimization for color image denoising," *Neurocomputing*, vol. 332, pp. 283–297, 2019.
[41] Y. Xu, L. Yu, H. Xu, H. Zhang, and T. Nguyen, "Vector sparse representation of color image using quaternion matrix analysis," *IEEE Trans. Image Process.*, vol. 24, no. 4, pp. 1315–1329, Apr. 2015.
[42] W. Dong, L. Zhang, G. Shi, and X. Wu, "Image deblurring and super-
resolution by adaptive sparse domain selection and adaptive regulariza-
tion," *IEEE Trans. Image Process.*, vol. 20, no. 7, pp. 1838–1857, Jul. 2011.
[43] J. K. Choi, C. Bao, and X. Zhang, "PET-MRI joint reconstruction by joint
sparsity based tight frame regularization," *SIAM J. Imag. Sci.*, vol. 11,
no. 2, pp. 1179–1204, 2018.
[44] J. Duan, Z. Pan, B. Zhang, W. Liu, and X.-C. Tai, "Fast algorithm for color
texture image inpainting using the non-local CTV model," *J. Glob. Optim.*,
vol. 62, pp. 853–876, 2015.
[45] S. Yan, J. Liu, H. Huang, and X.-C. Tai, "A dual EM algorithm for TV regu-
larized Gaussian mixture model in image segmentation," *Inverse Problems Imag.*, vol. 13, pp. 653–677, 2019.
[46] Y. Zhang and X. Zhang, "PET-MRI joint reconstruction with common
edge weighted total variation regularization," *Inverse Problems*, vol. 34,
no. 6, pp. 1–22, 2018.
[47] J. Cai, B. Dong, S. Osher, and Z. Shen, "Image restoration: Total varia-
tion, wavelet frames, and beyond," *J. Amer. Math. Soc.*, vol. 25, no. 4,
pp. 1033–1089, 2012.
[48] Y. Dong, T. Görner, and S. Kunis, "An algorithm for total variation regu-
larized photoacoustic imaging," *Adv. Comput. Math.*, vol. 41, no. 2,
pp. 423–438, 2015.
[49] Z. Jia, M. K. Ng, and W. Wang, "Color image restoration by saturation-
value total variation," *SIAM J. Imag. Sci.*, vol. 12, no. 2, pp. 972–1000,
2019.
[50] H. Hai, X. D. Qing, and Q. Ke, "A watermarking-based authentication and
image restoration in multimedia sensor networks," *Int. J. High Perform.
Comput. Netw.*, vol. 12, no. 1, pp. 65–73, 2018.
[51] C. Sánchez-Ferreira, L. Coelho, H. V. Ayala, M. C. Farias, and C. H.
Llanos, "Bio-inspired optimization algorithms for real underwater image
restoration," *Signal Process.: Image Commun.*, vol. 77, pp. 49–65, 2019.

522
523
524
525
526
527
528
529
530
531
532
533
534
535
536
537
538
539
540
541
542
543
544
545
546
547
548
549
550
551
552
553
554
555
556
557
558
559
560
561
562
563
564
565
566
567
568
569
570
571
572
573
574
575
576
577
578
579
580
581
582
583
584
585
586
587
588
589
590
591
592
593
594
595
596

- [52] S. W. Zamir *et al.*, “Learning enriched features for real image restoration and enhancement,” in *Proc. Eur. Conf. Comput. Vision (ECCV)*, 2020, pp. 492–511.
- [53] M. Zach and E. Kobler, “Real-world video restoration using Noise2Noise,” in *Proc. Joint Austrian Comput. Vis. Robot. Workshop. Verlag der Technischen Universität Graz*, 2020, pp. 145–150.
- [54] Y. Chen, Z. Jia, Y. Peng, and Y. Peng, “Robust dual-color watermarking based on quaternion singular value decomposition,” *IEEE Access*, vol. 8, pp. 30 628–30 642, 2020.
- [55] W. R. Hamilton, *Elements of Quaternions*. London: Longmans, Green, & Company, 1866.
- [56] Z. Jin, F. Li, and M. K. Ng, “A variational approach for image decolorization by variance maximization,” *SIAM J. Imag. Sci.*, vol. 7, no. 2, pp. 944–968, 2014.
- [57] D. Gabay and B. Mercier, “A dual algorithm for the solution of nonlinear variational problems via finite element approximations,” *Comput. Math. Appl.*, vol. 2, pp. 17–40, 1976.
- [58] L. Chen, X. Li, D. Sun, and K.-C. Toh, “On the equivalence of inexact proximal ALM and ADMM for a class of convex composite programming,” *Math. Program.*, vol. 185, pp. 111–161, 2021.
- [59] L. Chen, D. Sun, and K.-C. Toh, “A note on the convergence of ADMM for linearly constrained convex optimization problems,” *Comput. Optim. Appl.*, vol. 66, no. 2, pp. 327–343, 2017.
- [60] S. Boyd, N. Parikh, E. Chu, B. Peleato, and J. Eckstein, “Distributed optimization and statistical learning via the alternating direction method of multipliers,” *Found. Trends Mach. Learn.*, vol. 3, no. 1, pp. 1–122, 2011.
- [61] A. Ignatov *et al.*, “PIRM challenge on perceptual image enhancement on smartphones: Report,” in *Proc. Eur. Conf. Comput. Vis. Workshops*, 2019, pp. 1–18.
- [62] Y. Wang, J. Yang, W. Yin, and Y. Zhang, “A new alternating minimization algorithm for total variation image reconstruction,” *SIAM J. Imag. Sci.*, vol. 1, pp. 248–272, 2008.
- [63] S. Ono and I. Yamada, “Decorrelated vectorial total variation,” *Proc. IEEE Conf. Comput. Vis. Pattern Recognit.*, 2014, pp. 4090–4097.
- [64] J. Zhang, D. Zhao, and W. Gao, “Group-based sparse representation for image restoration,” *IEEE Trans. Image Process.*, vol. 23, no. 8, pp. 3336–3351, Aug. 2014.
- [65] N. Wang, W. Shi, C. Fan, and L. Lou, “An improved nonlocal sparse regularization-based image deblurring via novel similarity criteria,” *Int. J. Adv. Robot. Syst.*, vol. 15, pp. 1–18, 2018.
- [66] J.-J. Liu, Y. Lou, G. Ni, and T. Zeng, “An image sharpening operator combined with framelet for image deblurring,” *Inverse Problems*, vol. 36, no. 045015, pp. 1–27, 2020.
- [67] A. Danielyan, V. Katkovnik, and K. O. Egiazarian, “BM3D frames and variational image deblurring,” *IEEE Trans. Image Process.*, vol. 21, no. 4, pp. 1715–1728, Apr. 2012.
- [68] X. Zhang and B. Wandell, “A spatial extension of CIELAB for digital color-image reproduction,” *J. Soc. Inf. Display*, vol. 5, pp. 61–63, 1997.
- [69] Z. Wang, A. Bovik, H. R. Sheikh, and E. P. Simoncelli, “Image quality assessment: From error visibility to structural similarity,” *IEEE Trans. Image Process.*, vol. 13, no. 4, pp. 600–612, Apr. 2004.
- [70] A. Robertson *et al.*, “CIE recommendations on uniform color spaces, color-difference equations, and metric color terms,” *Color Res. Appl.*, vol. 2, no. 1, pp. 5–6, 1977.



Chaoyan Huang received the B.S. degree with the College of Mathematics and Computer Science, Anqing Normal University, Anqing, China, in 2019. She is currently working toward the M.S. degree with the School of Science, Nanjing University of Posts and Telecommunications, Nanjing, China. Her research interests include image processing, inverse problems, and machine learning.



Michael K. Ng received the B.Sc. and M.Phil. degrees from the University of Hong Kong, Hong Kong, in 1990 and 1992, respectively, and the Ph.D. degree from the Chinese University of Hong Kong, Hong Kong, in 1995. He is currently a Chair Professor with the Department of Mathematics, University of Hong Kong. His research interests include bioinformatics, image processing, scientific computing, and data mining.



Tingting Wu received the B.S. and Ph.D. degrees in mathematics from Hunan University, Changsha, China, in 2006 and 2011, respectively. From 2015 to 2018, she was a Postdoctoral Researcher with the School of Mathematical Sciences, Nanjing Normal University, Nanjing, China. From 2016 to 2017, she was a Research Fellow with Nanyang Technological University, Singapore. She is currently an Associate Professor with the School of Science, Nanjing University of Posts and Telecommunications, Nanjing, China. Her research interests include variational methods for image processing and computer vision, optimization methods and their applications in sparse recovery, and regularized inverse problems.



Tieyong Zeng received the B.S. degree from Peking University, Beijing, China, in 2000, the M.S. degree from École Polytechnique, Palaiseau, France, in 2004, and the Ph.D. degree from the University of Paris XIII, Paris, France, in 2007. He was a Postdoctoral Researcher with ENS de Cachan, Cachan, France, since 2007 to 2008, and an Assistant/Associate Professor with Hong Kong Baptist University, Hong Kong, since 2008 to 2018. He is currently a Professor with the Department of Mathematics, The Chinese University of Hong Kong, Hong Kong. His research interests include image processing, machine learning, and scientific computing.

Quaternions-Based Dictionary Learning and Saturation-Value Total Variation Regularization for Color Image Restoration

Chaoyan Huang^{ID}, Michael K. Ng^{ID}, Tingting Wu^{ID}, and Tieyong Zeng^{ID}

Abstract—Color image restoration is a critical task in imaging sciences. Most variational methods regard the color image as a Euclidean vector or the direct combination of three monochrome images and completely ignore the inherent color structures within channels. To better describe the relationship of color channels, we represent the color image as the so-called pure quaternion matrix. Note that the celebrated dictionary learning method has attracted considerable attention for image recovery in the past decade. Following this idea, we propose a novel quaternion-based color image recovery method. This model combines the advantages of dictionary learning and the total variation method for color image restoration. The new strategy used in the proposed model manages to handle the color image restoration problem in the quaternion space. Moreover, the new proposed model can be easily solved by the classical alternating direction method of multipliers (ADMM) algorithm. Numerical results demonstrate clearly that the performance of our proposed dictionary learning method is better than some state-of-the-art color image dictionary learning and total variation methods in terms of some criteria and visual quality.

Index Terms—Dictionary learning, image restoration, pure quaternion, total variation.

I. INTRODUCTION

COLOR image restoration aims to recover a clean image from the degraded observation. In the processing of generating, transmission, and storage, the color image will be unavoidably degraded by noise and blur. As images are essential

Manuscript received April 14, 2021; revised July 13, 2021; accepted August 18, 2021. This work was supported in part by the National Key R&D Program of China under Grant 2021YFE0203700, in part by NSFC/RGC N_CUHK 415/19, RGC 14300219, 14302920, and 14301121, in part by the CUHK Direct grant for Research under Grants 4053405 and 4053460, in part by the Graduate Student Scientific Research Innovation Project of Jiangsu Province, 2020, under Grant KYCX20_0788, in part by HKRGC GRF under Grants 12300218, 12300519, 17201020, and 17300021, in part by the Natural Science Foundation of China under Grants 61971234 and 11501301, in part by the 1311 Talent Plan of NUPT, the QingLan Project for Colleges and Universities of Jiangsu Province. The associate editor coordinating the review of this manuscript and approving it for publication was Dr. Jiale (Jerry) Shen. (*Corresponding author: Tingting Wu.*)

Chaoyan Huang and Tingting Wu are with the School of Science, Nanjing University of Posts and Telecommunications, Nanjing 210003, China (e-mail: 1019081805@njupt.edu.cn; wutt@njupt.edu.cn).

Michael K. Ng is with the Department of Mathematics, The University of Hong Kong, Hong Kong (e-mail: mng@maths.hku.hk).

Tieyong Zeng is with the Department of Mathematics, The Chinese University of Hong Kong Shatin, Hong Kong (e-mail: zeng@math.cuhk.edu.hk).

Color versions of one or more figures in this article are available at <https://doi.org/10.1109/TMM.2021.3107162>.

Digital Object Identifier 10.1109/TMM.2021.3107162

in various fields such as biomedical imaging, microscopy, astronomical imaging, and multimedia processing, it is critical to restoring the sharp image from the degraded observation.

The color image processing is the extension of gray image restoration. Since color image restoration is a typical ill-posed problem, recovering the degraded image is rather challenging. In the literature, there are many excellent methods for gray image restoration. Rudin, Osher, and Fatemi [1] proposed the total variation (TV)-based method to handle the image denoising problem. Later, the TV-based model was extended by many researchers to tackle the image restoration problem, such as [2], [3]. In [4], the reliable image recovery results were generated by the dictionary learning (DL)-based method. Zeng *et al.* [5] applied the DL-based method for image denoising and yielded competitive results. The DL-based method, first introduced by Olshausen and Field [6] and continued by Elad *et al.* [7]–[9], has been applied to various tasks of image processing, such as image restoration [10], [11], image inpainting [12], [13], image recognition [14], [15], image compression [16], image classification [17], and object detection [18]. Recently, the machine learning-based method has received significant attention in image processing and has good results in image restoration. For example, Jin *et al.* [19] proposed a flexible deep convolutional neural networks (CNN) framework for image restoration. Mou *et al.* [20] restored the image with the collaborative attention network (COLA-Net). In [21], Popyan, Romano, and Elad built a nice connection between CNN and DL, which provided a new interpretation of CNN. Moreover, [22] also gave the theoretical guarantees for convolutional sparse coding. However, the integration of the DL-based method with the most recent advanced tools in image processing is still an open question.

As an important branch of image processing, DL aims at searching for a suitable dictionary where the trained data has sparse representation [23]–[26]. By minimizing the reconstruction error of the training data, the dictionary learning method can take full advantage of the sample information [27], [28]. By giving the following assumption: an image patch $\mathbf{u}_0 \in \mathbb{R}^m$ is approximately sparse under some dictionary $\mathbf{D} \in \mathbb{R}^{m \times k}$; the linear measurement $\mathbf{g}_0 = \mathbf{u}_0 + \mathbf{b}_0$ where \mathbf{b}_0 is the noise following some statistical distributions; estimating the original image patch \mathbf{u}_0 as $\mathbf{u}_0 \approx \mathbf{D}\mathbf{a}$. Then we can get \mathbf{u}_0 by solving

$$\min_{\mathbf{a}} \|\mathbf{a}\|_0, \text{s.t. } \|\mathbf{g}_0 - \mathbf{D}\mathbf{a}\|_2^2 \leq \epsilon, \quad (1)$$

73 where $\|\cdot\|_0$ denotes the ℓ_0 -norm which counts the number
 74 of non-zero elements; $\|\cdot\|_2$ represents the ℓ_2 norm, i.e.,
 75 $\|x\|_2 = \sqrt{\sum_{t=1}^l x_t^2}$ with $x = \{x_1, x_2, \dots, x_l\}$; \mathbf{a} represents the sparse coefficient vector; and $\epsilon \geq 0$ is a parameter with respect
 76 to the noise level. Once we have obtained the solution \mathbf{a} of (1),
 77 with the given dictionary \mathbf{D} , the original image patch \mathbf{u}_0 can be
 78 estimated by $\mathbf{u}_0 = \mathbf{D}\mathbf{a}$.

79 The choice of the dictionary \mathbf{D} has a significant influence
 80 on the performance of the image restoration. The dictionary \mathbf{D}
 81 can be either given or learned from observed images [29], [30].
 82 For the predetermined dictionary, such as curvelets, wavelets,
 83 and discrete cosine transforms (DCT), their computational per-
 84 formances are always faster than the learned ones. However,
 85 the predetermined dictionary is not adapted to the degraded
 86 images [4]. A trained dictionary containing the prior informa-
 87 tion can better fit the images and significantly improve recovery
 88 quality [31], [32]. Among the learned dictionaries, Ma, Yu, and
 89 Zeng [33] learned the dictionary from the corresponding de-
 90 graded image and led to competitive performance in impulse
 91 noise removal. Chen *et al.* [34] learned a compact dictionary
 92 from original contaminated samples for face recognition. In [35],
 93 the authors applied a set of image patches to train a dictionary for
 94 spectral computed tomography (CT) material decomposition.
 95 In [36], the dictionary is trained using image patches for image
 96 denoising under mixed noise. The methods above have good re-
 97 sults in their tasks. However, the dictionary can contain more
 98 prior information. Inspired by the deep learning-based method,
 99 we train the dictionary by using a set of color images.

100 Considering the color information of an image is indispens-
 101 able, and color images have wide applications in our lives. Many
 102 researchers turned to tackle color image restoration. However,
 103 most of them simply apply the techniques of the gray image to
 104 color image restoration. The dictionary learning model can well
 105 handle the gray image in [7] but generate color distribution when
 106 denoising the color image in [9]. Therefore, simply applying the
 107 gray image-based method to the color image seems not suitable.
 108 Pei and Cheng [37] claimed that there are inner-relationships be-
 109 tween the red, green, and blue (RGB) channels of color images.
 110 They represented the color image with a quaternion matrix and
 111 had better results than those used in the gray image. Recently,
 112 many works paid a lot of attention to quaternion representation.
 113 Li, Zhou, and Zhang [38] used the quaternion non-local total
 114 variation regularizer for color image denoising. Their results
 115 are better than the real-valued non-local total variation-based
 116 methods. In [39] and [40], the authors extended the low-rank
 117 matrix approximation into the quaternion domain and achieved
 118 better color image denoising results than the real-valued low
 119 rank-based methods. Xu *et al.* [41] applied the DL with quater-
 120 nion for color image denoising, inpainting, and super-resolution.
 121 They achieved good results by representing color images with
 122 the quaternion matrix. A quaternion has three imaginary parts
 123 and one real part. We consider that representing a color image
 124 with three imaginary parts is better than simply regarding the
 125 color image as a union of three independent channels.

126 Although the dictionary method achieves good results, there
 127 is still room for improvement, i.e., they cannot preserve image
 128 edges well [33]. Moreover, the simple patch-based approach will

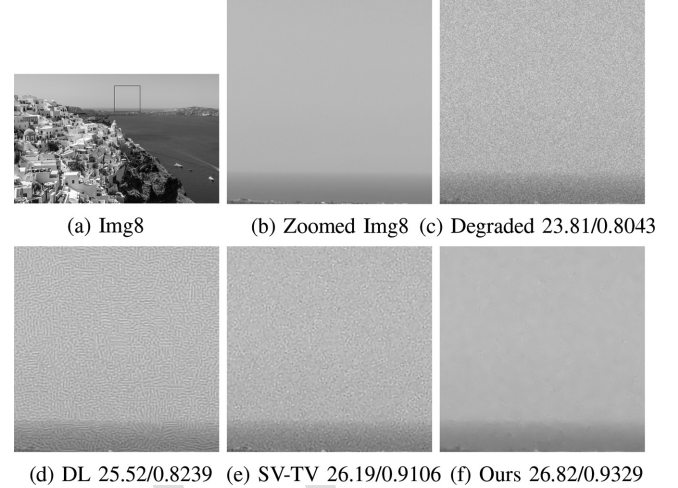


Fig. 1. The comparison of different restoration methods with visual results and PSNR/SSIM values. (a) Original image; (b) The zoomed part of Img8; (c) The zoomed part of the degraded image with Gaussian blur (15,1) and Gaussian noise level $\sigma = 12.75$; The zoomed part of images reconstructed by: (d) the dictionary learning method; (e) the SV-TV method; (f) our method.

introduce artifacts in the deblurring problem [42], [43]. Since the TV regularizer has attractive properties, i.e., convex and better sharp edge preservation [44]–[46], the TV- ℓ_1 model has been widely applied to image deblurring and denoising tasks [47], [48]. Recently, Jia, Ng, and Wang [49] proposed a TV model in HSV color space, named SV-TV, which can remove blur and noise effectively. Their study offers some important insights into our research. A brief review of the SV-TV regularizer is given in Section II.B.

In this paper, we propose a new color image restoration method with quaternion-based dictionary learning and SV-TV regularizers. As aforementioned, dictionary learning with quaternion representation can better preserve the inherent structure of the color image. Moreover, the total variation regularizer in HSV color space has better performance. Many excellent approaches have considered color image restoration with the TV-based method, non-local means-based method, or the DL-based method. However, the combination of both TV and quaternion-based DL has not been addressed in color image restoration. Moreover, due to the complexity, the quaternion-based techniques have rarely been applied in color image restoration. In this paper, we first apply the quaternion-based dictionary learning method with the SV-TV regularizer to deblur and denoise an image simultaneously. Inspired by the machine learning-based method, we train the dictionary with a large dataset. The trained dictionary can be seen as a prior. Furthermore, we do not need to train the dictionary corresponding to the input image, which saves the restoration time dramatically compared with those dictionary learning-based methods. Notably, the proposed combination model can be regarded as a general and flexible framework. Indeed, whenever necessary, one can also adopt other advanced regularizers or blocks to generate better results. In this paper, we focus on image restoration by combining dictionary learning and SV-TV regularizers for efficiency. Fig. 1 shows the comparison of different restoration methods. It is clear that the DL-based method generates great artifacts in Fig. 1(d). For the

SV-TV method, we find that some noises remained in Fig. 1(e). Our approach combines these two regularizers for color image restoration and generates a great result in Fig. 1(f). Hence, the image that we recovered has the highest numerical result and visual quality.

Indeed, the sparse representation prior is pretty good at recovering the local features in the image, and the TV term helps stabilize the restored results. Combining pure quaternion-based DL and TV regularizers, we propose a new color image restoration method. The main contributions of our method are as follows:

- Unlike the traditional color image processing, which regards the color image as the vector or the combination of monochrome images and completely ignores the inherent color structures, we represent a color image with the pure quaternion. Both denoising and deblurring are conducted to recover a color image. Due to the special calculation rules, the inner relationship among the multiple channels can be well preserved.
- We propose a new image restoration method combining quaternion-based DL and SV-TV regularizers to recover the degraded color images and achieve more competitive color image restoration results than existing methods.
- For the numerical implementation, we train a dictionary with a large dataset and then fix the trained dictionary. Based on this strategy, there is no need to train a new corresponding dictionary for each image. Meanwhile, our pre-learned dictionary can also fit the degraded images in the processing of image restoration.

Additionally, the proposed method can be used in many real applications, including multimedia computing [50], image restoration [51], [52], video enhancement [53].

The paper is organized as follows. Section II reviews the basic concept of the quaternion, the SV-TV regularization, and the classical alternating direction method of multipliers (ADMM) algorithm. The proposed method is displayed in Section III, and experimental results are in Section IV. Finally, the conclusions follow in Section V.

II. QUATERNION AND SV-TV REGULARIZATION

A. Quaternion

The quaternion matrix is proven to be a better representation for color image restoration than the real-valued matrix [54]. The quaternion was first introduced by Hamilton [55]. Assume that \mathbb{H} is a quaternion space, let $\mathbf{u}(x, y) \in \mathbb{H}$ be a quaternion, then

$$\mathbf{u}(x, y) = u_0(x, y) + u_1(x, y)\mathbf{i} + u_2(x, y)\mathbf{j} + u_3(x, y)\mathbf{k},$$

where $u_0(x, y) \in \mathbb{R}$ is the real part, $u_1(x, y)$, $u_2(x, y)$, $u_3(x, y) \in \mathbb{R}$ are the imaginary parts, and $\mathbf{i}, \mathbf{j}, \mathbf{k}$ are three fundamental quaternion units satisfying the following quaternion rules

$$\mathbf{i}^2 = \mathbf{j}^2 = \mathbf{k}^2 = \mathbf{ijk} = -1,$$

$$\mathbf{ij} = -\mathbf{ji} = \mathbf{k}, \mathbf{jk} = -\mathbf{kj} = \mathbf{i}, \mathbf{ki} = -\mathbf{ik} = \mathbf{j}.$$

Similar to complex space, if the real part $u_0(x, y) = 0$, then $\mathbf{u}(x, y)$ is called a pure quaternion. As the color image has three



Fig. 2. Color image with quaternion representation.

channels (R, G, B), we can represent a color image with the imaginary parts of the quaternion, i.e., denoting the color image as the pure quaternion

$$\mathbf{u}(x, y) = u_r(x, y)\mathbf{i} + u_g(x, y)\mathbf{j} + u_b(x, y)\mathbf{k},$$

here (x, y) refers to the pixel location of a color image \mathbf{u} , and $u_r(x, y)$, $u_g(x, y)$, $u_b(x, y)$ are the RGB channels, respectively. Fig. 2 shows how the quaternion represents the color image.

B. SV-TV Regularization

Rudin, Osher, and Fatemi first proposed the TV regularization [1] for gray image restoration, which can preserve the edge of images. The TV term can suppress artifacts generated by the patch-based methods [56]. Given an observed image \mathbf{g} , the TV model can be written as

$$\mathbf{u} = \arg \min_{\mathbf{u}} \eta \|\nabla \mathbf{u}\|_1 + \frac{1}{2} \|\mathbf{g} - \mathbf{H} * \mathbf{u}\|_2^2, \quad (2)$$

where \mathbf{u} is the latent image, \mathbf{H} is a given blur operator, $*$ is the convolutional operation, η is the positive parameter that balance the different terms, $\frac{1}{2} \|\mathbf{g} - \mathbf{H} * \mathbf{u}\|_2^2$ is the fidelity term,

$$\|\nabla \mathbf{u}\|_1 = \sum_{i=1}^m \sum_{j=1}^n \sqrt{(\mathbf{d}_x \mathbf{u})_{ij}^2 + (\mathbf{d}_y \mathbf{u})_{ij}^2}$$

is the TV regularization term, here two discrete differential operators are introduced as

$$\begin{cases} (\mathbf{d}_x \mathbf{u})_{ij} = \mathbf{u}(i, j) - \mathbf{u}(i-1, j), \\ (\mathbf{d}_y \mathbf{u})_{ij} = \mathbf{u}(i, j) - \mathbf{u}(i, j-1). \end{cases}$$

The SV-TV regularization is introduced by Jia *et al.* [49], which is the extension of TV regularization. The SV-TV can be expressed as

$$\min_{\mathbf{u}} \eta \text{SV-TV}(\mathbf{u}) + \frac{1}{2} \|\mathbf{g} - \mathbf{H} * \mathbf{u}\|_2^2, \quad (3)$$

where

$$\begin{aligned} \text{SV-TV}(\mathbf{u}) = & \sum_{i=1}^m \sum_{j=1}^n \left(\sqrt{|(\mathbf{d}_x \mathbf{u})_{ij}|_s^2 + |(\mathbf{d}_y \mathbf{u})_{ij}|_s^2} \right. \\ & \left. + \alpha \sqrt{|(\mathbf{d}_x \mathbf{u})_{ij}|_v^2 + |(\mathbf{d}_y \mathbf{u})_{ij}|_v^2} \right), \end{aligned} \quad (4)$$

here $\alpha > 0$ is the weight of the value component. The norm $|\cdot|_s$ and $|\cdot|_v$ are defined as

$$\begin{aligned} |(\mathbf{d}_x \mathbf{u})_{ij}|_s &= \frac{1}{3} \|\mathbf{C}(\mathbf{d}_x \mathbf{u})_{ij}^T\|_2, \\ |(\mathbf{d}_y \mathbf{u})_{ij}|_s &= \frac{1}{3} \|\mathbf{C}(\mathbf{d}_y \mathbf{u})_{ij}^T\|_2, \\ |(\mathbf{d}_x \mathbf{u})_{ij}|_v &= \frac{1}{\sqrt{3}} |(\mathbf{d}_x u_r)_{ij} + (\mathbf{d}_x u_g)_{ij} + (\mathbf{d}_x u_b)_{ij}|, \\ |(\mathbf{d}_y \mathbf{u})_{ij}|_v &= \frac{1}{\sqrt{3}} |(\mathbf{d}_y u_r)_{ij} + (\mathbf{d}_y u_g)_{ij} + (\mathbf{d}_y u_b)_{ij}|, \end{aligned} \quad (5)$$

where $\mathbf{C} = \begin{bmatrix} 2 & -1 & -1 \\ -1 & 2 & -1 \\ -1 & -1 & 2 \end{bmatrix}$. We refer the interested readers

to [49] for a more comprehensive review of the SV-TV regularizer. Our proposed model applies the SV-TV regularizer to denote the piecewise-constant image part, such that the artifacts accompanied with the patch-based method can be removed.

C. ADMM Algorithm

The alternating direction method of multipliers (ADMM) algorithm [57]–[59] aims to solve the problem with the following form

$$\min_x f(x) + h(Bx). \quad (6)$$

Here, $f(x)$ and $h(Bx)$ are two convex functions, B is a constant. Let $z = Bx$, the augmented Lagrangian of (6) is

$$L_\delta(x, z; y) = f(x) + h(z) + \langle y, Bx - z \rangle + \frac{\delta}{2} \|Bx - z\|_2^2,$$

where y is called the Lagrange multiplier and δ is the penalty parameter. The ADMM algorithm consists of the iterations as follows

$$\begin{aligned} x &= \arg \min_x f(x) + \langle y, Bx - z \rangle + \frac{\delta}{2} \|Bx - z\|_2^2, \\ z &= \arg \min_z h(z) + \langle y, Bx - z \rangle + \frac{\delta}{2} \|Bx - z\|_2^2, \\ y &= y + \delta(Bx - z). \end{aligned}$$

By alternating updates x and z subproblems and the Lagrange multiplier y , the optimal solution x with guaranteed convergence is obtained. One can have a detailed comprehending in [60], the Matlab examples and related works can be found in https://stanford.edu/boyd/papers/admm_distr_stats.html.

III. OUR METHOD

In this section, we first give the proposed method. Then provide the strategy of training the dictionary. The numerical algorithm of the proposed model is also presented. Finally, we give the computation complexity of the proposed algorithm.

TABLE I
NOTATIONS USED THROUGH THE PAPER

\mathbf{u}_0	the image patch
\mathbf{D}	the dictionary
\mathbf{b}_0	the Gaussian noise
\mathbf{a}	the sparse coefficient vector
a_{ij}	the sparse coefficient for the patch located at (i, j)
\mathbf{A}	the set of \mathbf{a}_{ij}
ϵ	the parameter with respect to noise level
\mathbb{H} and \mathbb{R}	the quaternion space and the real space
$w_0(x, y)$	the real part of a quaternion function
$w_t(x, y)$	the imaginary part of a quaternion function, $t = 1, 2, 3$
$u_k(x, y)$	the RGB part of an image, $k = r, g, b$
$\mathbf{i}, \mathbf{j}, \mathbf{k}$	the fundamental quaternion units
$\mathbf{u}(x, y)$	the quaternion function
\mathbf{u}	the latent image
\mathbf{g}	the observed image
η, α, λ	the positive parameter that balance the different term
$\ \cdot\ _t$	the ℓ_t -norm, $t = 0, 1, 2$
∇	the gradient operator
$\ \nabla \mathbf{u}\ _1$	the TV term
$*$	the convolutional operation
\mathbf{H}	the blur operator
$(\mathbf{d}_x \mathbf{u})_{ij}$	discrete differential operator of x orientation in location (i, j)
$(\mathbf{d}_y \mathbf{u})_{ij}$	discrete differential operator of y orientation in location (i, j)
$ \cdot _s$ and $ \cdot _v$	the s -norm and the v -norm
\mathbf{P}, \mathbf{P}_0 and \mathbf{P}_0^T	orthogonal matrices and the conjugate transpose of \mathbf{P}_0
\mathbf{J}	the singular value matrix of \mathbf{C}
\mathbf{q}	the linear transformation of \mathbf{u}
\mathbf{q}_t	three components of \mathbf{q} , $t = 1, 2, 3$
ρ_{ij}	the positive weight for patch at location (i, j)
\mathcal{R}_{ij}	the extract operator in location (i, j)
$\tilde{\mathbf{H}}, \tilde{\mathbf{g}}, \tilde{\mathbf{D}}, \tilde{\mathbf{a}}_{ij}$	the corresponding linear transformation with \mathbf{P}
$\mathbf{w}_t^x, \mathbf{w}_t^y$	auxiliary variables in ADMM algorithm, $t = 1, 2, 3$
τ_t^x, τ_t^y	Lagrangian multipliers $t = 1, 2, 3$
β	the penalty parameter

A. Proposed Scheme

Given an observed image \mathbf{g} and the blur operator \mathbf{H} , the proposed model is given as

$$\begin{aligned} \min_{\mathbf{a}_{ij}, \mathbf{u}} \lambda \|\mathbf{g} - \mathbf{H} \star \mathbf{u}\|_2^2 + \eta \text{SV-TV}(\mathbf{u}) \\ + \sum_{i,j} \rho_{ij} \|\mathbf{a}_{ij}\|_0 + \sum_{i,j} \|\mathbf{D} \mathbf{a}_{ij} - \mathcal{R}_{ij} \mathbf{u}\|_2^2, \end{aligned} \quad (7)$$

where λ and η are two positive parameters, \mathbf{u} is the ideal latent image. The second term $\text{SV-TV}(\mathbf{u})$ is the regularizer proposed in the HSV color space. The last two terms are the dictionary learning model, where ρ_{ij} is the positive patch-specific weight, the binary matrix \mathcal{R}_{ij} extracts the local patch in an image, \mathbf{D} is a pre-learned dictionary, and \mathbf{a}_{ij} is the sparse coefficient vector. The set of \mathbf{a}_{ij} is denoted as \mathbf{A} . Fig. 3 summarized our approach with the pre-learned dictionary. Table I gives a list of notations used in this paper.

B. Learning the Dictionary With K-QSVD Algorithm

The last two terms in (7) are corresponding to the above-mentioned sparsity assumption (1) (for some dictionary). In the dictionary learning part, the training images are collected from the training set of the DIV2K Dataset [61]. We download 800 training images and crop them into small patches of size 8×8 . We then learned a dictionary from these image patches with the

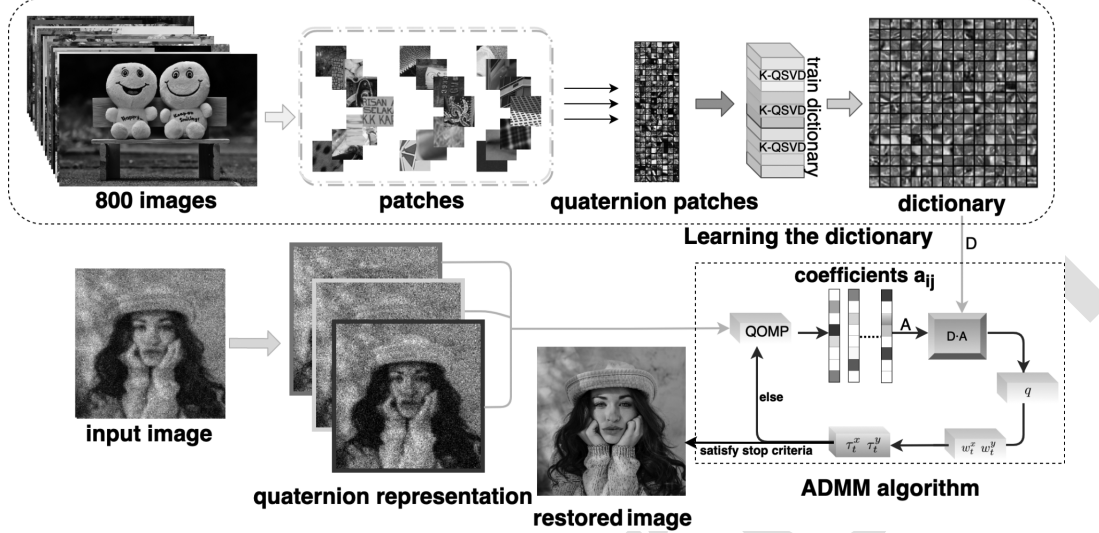


Fig. 3. The flowchart of our method.

generalized k-means clustering for quaternion singular value decomposition (K-QSVD) algorithm¹ [41]. The learned dictionary D is with the size of $64 \times 256 \times 4$. It takes 291.75 seconds in Matlab R2020a under macOS Catalina 10.15.4 with a 1.40 GHz CPU and 8 GB memory. The number of nonzero entries in a_{ij} is called the sparsity level of a_{ij} . In this paper, the sparsity level is set to be 5, which is the default value in the K-QSVD algorithm. After the dictionary is learned, we fix it for all image restoration. Fig. 3 contains the processing of dictionary training.

C. Numerical Algorithm of the Proposed Model (7)

To better solve the proposed model, we first perform a linear transformation. Since the component of SV-TV ((4)) satisfies the (5). Given the orthogonal decomposition of C , i.e., $C = P_0^T J P_0$, where P_0 is the orthogonal matrix and

$$J = \begin{bmatrix} 3 & 0 & 0 \\ 0 & 3 & 0 \\ 0 & 0 & 0 \end{bmatrix}, P_0 = \begin{bmatrix} \frac{1}{\sqrt{2}} & \frac{-1}{\sqrt{2}} & 0 \\ \frac{1}{\sqrt{6}} & \frac{1}{\sqrt{6}} & \frac{-2}{\sqrt{6}} \\ \frac{1}{\sqrt{3}} & \frac{1}{\sqrt{3}} & \frac{1}{\sqrt{3}} \end{bmatrix}, \quad (8)$$

following (8), by doing the linear transformation of u , we have

$$q = \begin{bmatrix} q_1(x, y) \\ q_2(x, y) \\ q_3(x, y) \end{bmatrix} = P u = P \begin{bmatrix} u_r(x, y) \\ u_g(x, y) \\ u_b(x, y) \end{bmatrix}, \quad (9)$$

here

$$P = \begin{bmatrix} \frac{1}{\sqrt{2}} I & \frac{-1}{\sqrt{2}} I & 0 \\ \frac{1}{\sqrt{6}} I & \frac{1}{\sqrt{6}} I & \frac{-2}{\sqrt{6}} I \\ \frac{1}{\sqrt{3}} I & \frac{1}{\sqrt{3}} I & \frac{1}{\sqrt{3}} I \end{bmatrix},$$

and I is the identity matrix. With the fixed P , by doing the linear transformation, we set $\tilde{H} = PHP^T$, $\tilde{g} = Pg$, $\tilde{D} = PD$,

¹The code of the K-QSVD algorithm can be found in [Online]. Available: <https://lichengunc.github.io/>.

$\tilde{a}_{ij} = a_{ij}$. The objective function (7) is reformulated as

$$\begin{aligned} \min_{\tilde{a}_{ij}, q} & \lambda \|\tilde{H} * q - \tilde{g}\|_2^2 + \eta \text{SV-TV}(q) \\ & + \sum_{i,j} \rho_{ij} \|\tilde{a}_{ij}\|_0 + \sum_{i,j} \|\tilde{D} \tilde{a}_{ij} - \mathcal{R}_{ij} q\|_2^2, \end{aligned} \quad (10)$$

where

$$\begin{aligned} \text{SV-TV}(q) = & \sum_{i=1}^m \sum_{j=1}^n (\alpha \sqrt{(\mathbf{d}_x q_3)_{ij}^2 + (\mathbf{d}_y q_3)_{ij}^2} \\ & + \sqrt{(\mathbf{d}_x q_1)_{ij}^2 + (\mathbf{d}_x q_2)_{ij}^2 + (\mathbf{d}_y q_1)_{ij}^2 + (\mathbf{d}_y q_2)_{ij}^2}). \end{aligned} \quad (11)$$

Following previous works [41], [49], we can establish the optimization scheme based on the ADMM approach [57]–[59]. According to II-C, by introducing auxiliary variables w_t^x , w_t^y , Lagrangian multipliers τ_t^x and τ_t^y ($t = 1, 2, 3$), and a penalty parameter $\beta > 0$, we have the augmented Lagrangian of the proposed model as follows

$$\begin{aligned} L_\beta(\tilde{a}_{ij}, q, w_t^x, w_t^y; \tau_t^x, \tau_t^y) = & \sum_{i=1}^m \sum_{j=1}^n \left(\lambda \|\tilde{H} * q - \tilde{g}\|_2^2 + \rho_{ij} \|\tilde{a}_{ij}\|_0 + \|\tilde{D} \tilde{a}_{ij} - \mathcal{R}_{ij} q\|_2^2 \right. \\ & + \eta \left(\sqrt{|(w_1^x)_{ij}|^2 + |(w_2^x)_{ij}|^2 + |(w_1^y)_{ij}|^2 + |(w_2^y)_{ij}|^2} \right. \\ & \left. + \alpha \sqrt{|(w_3^x)_{ij}|^2 + |(w_3^y)_{ij}|^2} \right) + \sum_{t=1}^3 \left(\langle \tau_t^x, (w_t^x - \mathbf{d}_x q_t)_{ij} \rangle \right. \\ & \left. + \langle \tau_t^y, (w_t^y - \mathbf{d}_y q_t)_{ij} \rangle + \frac{\beta}{2} \|(w_t^x - \mathbf{d}_x q_t)_{ij}\|^2 \right. \\ & \left. + \frac{\beta}{2} \|(w_t^y - \mathbf{d}_y q_t)_{ij}\|^2 \right). \end{aligned} \quad (12)$$

Then the solution is derived by alternatively solving the following three subproblems.

309

- $\tilde{\mathbf{a}}_{ij}$ -subproblem

$$\min_{\tilde{\mathbf{a}}_{ij}} \sum_{i=1}^m \sum_{j=1}^n (\rho_{ij} \|\tilde{\mathbf{a}}_{ij}\|_0 + \|\tilde{\mathbf{D}}\tilde{\mathbf{a}}_{ij} - \mathcal{R}_{ij}\mathbf{q}\|_2^2), \quad (13)$$

310 following (1), given an observed image \mathbf{g} , the corresponding coefficient vectors \mathbf{a}_{ij} can be obtained. We apply the quaternion orthogonal matching pursuit (QOMP) algorithm² to get \mathbf{a}_{ij} .

- q-subproblem

$$\begin{aligned} \min_{\mathbf{q}} \lambda \|\tilde{\mathbf{H}} \star \mathbf{q} - \tilde{\mathbf{g}}\|_2^2 + \sum_{i=1}^m \sum_{j=1}^n & \|\tilde{\mathbf{D}}\tilde{\mathbf{a}}_{ij} - \mathcal{R}_{ij}\mathbf{q}\|_2^2 \\ & + \sum_{t=1}^3 (\langle \tau_t^x, (\mathbf{w}_t^x - \mathbf{d}_x \mathbf{q}_t)_{ij} \rangle + \langle \tau_t^y, (\mathbf{w}_t^y - \mathbf{d}_y \mathbf{q}_t)_{ij} \rangle) \\ & + \frac{\beta}{2} \|(\mathbf{w}_t^x - \mathbf{d}_x \mathbf{q}_t)_{ij}\|_2^2 + \frac{\beta}{2} \|(\mathbf{w}_t^y - \mathbf{d}_y \mathbf{q}_t)_{ij}\|_2^2, \end{aligned} \quad (14)$$

315 then the q-subproblem has a close form solution

$$\mathbf{q} = \frac{2\lambda \tilde{\mathbf{H}}^T \tilde{\mathbf{g}} + 2 \sum_{i,j} \mathcal{R}_{ij}^T \tilde{\mathbf{D}}\tilde{\mathbf{a}}_{ij} + \Xi}{2\lambda \tilde{\mathbf{H}}^T \tilde{\mathbf{H}} + 2 \sum_{i,j} \mathcal{R}_{ij}^T \mathcal{R}_{ij} + \beta(\mathbf{d}_x^T \mathbf{d}_x + \mathbf{d}_y^T \mathbf{d}_y)}, \quad (15)$$

316 where $\Xi = \sum_{t=1}^3 (\tau_t^x \mathbf{d}_x + \tau_t^y \mathbf{d}_y + \beta(\mathbf{d}_x^T \mathbf{w}_t^x + \mathbf{d}_y^T \mathbf{w}_t^y))$.

- \mathbf{w}_t^x and \mathbf{w}_t^y -subproblem ($t = 1, 2, 3$)

317 It is a typical problem that can be solved by the soft shrinkage algorithm [62]. According to the soft shrinkage algorithm, we have the solution of \mathbf{w}_t^x and \mathbf{w}_t^y as follows

$$\begin{aligned} \mathbf{w}_1^x &= \max(s_1 - \frac{\eta}{\beta}, 0) \frac{\mathbf{d}_1^x - \mathbf{w}_1^x/\beta}{s_1}, \\ \mathbf{w}_1^y &= \max(s_1 - \frac{\eta}{\beta}, 0) \frac{\mathbf{d}_1^y - \mathbf{w}_1^y/\beta}{s_1}, \\ \mathbf{w}_2^x &= \max(s_1 - \frac{\eta}{\beta}, 0) \frac{\mathbf{d}_2^x - \mathbf{w}_2^x/\beta}{s_1}, \\ \mathbf{w}_2^y &= \max(s_1 - \frac{\eta}{\beta}, 0) \frac{\mathbf{d}_2^y - \mathbf{w}_2^y/\beta}{s_1}, \\ \mathbf{w}_3^x &= \max(s_2 - \frac{\eta\alpha}{\beta}, 0) \frac{\mathbf{d}_3^x - \mathbf{w}_3^x/\beta}{s_2}, \\ \mathbf{w}_3^y &= \max(s_2 - \frac{\eta\alpha}{\beta}, 0) \frac{\mathbf{d}_3^y - \mathbf{w}_3^y/\beta}{s_2}, \end{aligned} \quad (16)$$

321 where

$$\begin{aligned} s_1 &= \sqrt{\sum_{t=1}^2 (\mathbf{d}_x - \frac{\mathbf{w}_t^x}{\beta})^2 + (\mathbf{d}_y - \frac{\mathbf{w}_t^y}{\beta})^2}, \\ s_2 &= \sqrt{(\mathbf{d}_x - \frac{\mathbf{w}_3^x}{\beta})^2 + (\mathbf{d}_y - \frac{\mathbf{w}_3^y}{\beta})^2}. \end{aligned} \quad (17)$$

- 322 • τ_t^x and τ_t^y -subproblem ($t = 1, 2, 3$)

²The code of the QOMP algorithm can be found in [Online]. Available: <https://lichengunc.github.io/>.

Algorithm 1: Our algorithm for image Restoration.

Initialization Represent color image with quaternion matrix. Given the pre-learned dictionary \mathbf{D} and the orthogonal matrix \mathbf{P} . Set $\mathbf{u} = \mathbf{g}$. Choose parameters $\lambda, \eta, \alpha, \beta$. Set the maximum iteration T .

for iteration=1 to T **do**

- Update $\tilde{\mathbf{a}}_{ij}$ with (13);
- Update \mathbf{q} using (15);
- Update \mathbf{w}_t^x and \mathbf{w}_t^y using (16);
- Update τ_t^x and τ_t^y using (18);
- $T = T + 1$.

end for

return $\mathbf{u} = \mathbf{P}^{-1}\mathbf{q}$.



Fig. 4. Ground-truth images.

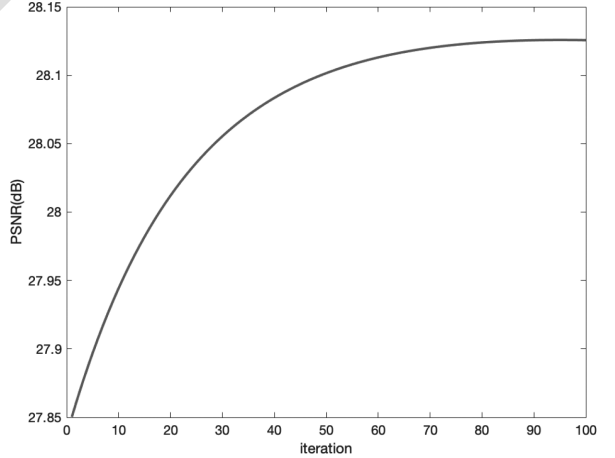


Fig. 5. PSNR values of results recovered from Img6 with ‘degraded=fspecial(‘Gaussian’,15,1)+noise’ by the proposed method.

323 The Lagrange multipliers are updated as follows.

$$\tau_t^x = \tau_t^x + \beta(\mathbf{w}_t^x - \mathbf{d}_x), \quad \tau_t^y = \tau_t^y + \beta(\mathbf{w}_t^y - \mathbf{d}_y). \quad (18)$$

324 By iterating \mathbf{a}_{ij} , \mathbf{q} , \mathbf{w}_t^x , and \mathbf{w}_t^y -subproblems and Lagrange 325 multipliers τ_t^x and τ_t^y ($t = 1, 2, 3$) with Eqs. (13)-(17), the 326 optimal solution \mathbf{q} is obtained. Since \mathbf{P} is an orthogonal matrix, 327 we can get the solution \mathbf{u} from (9). Our optimization scheme is 328 summarized in Algorithm 1.

D. Computation Complexity

329 The computation complexity also plays an important role in 330 determining the final performance of the proposed framework. 331 Suppose that we have M samples with dimension $m \times n \times 3$ 332

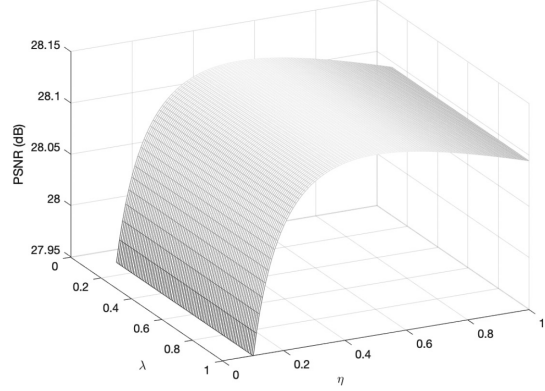
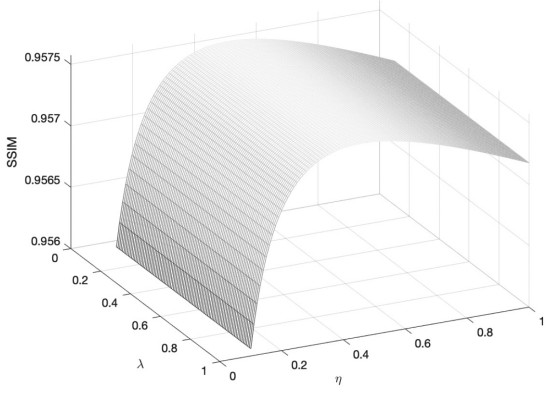
(a) PSNR values along with η and λ .(b) SSIM values along with η and λ .

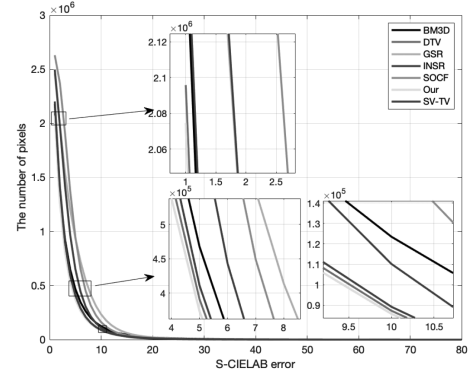
Fig. 6. Restoration results of Img6 with different parameters.

333 corresponding to color patches. The dictionary size is $m \times n \times$
 334 $3 \times K$, where K is the number of atoms. The sparsity constraint
 335 is $3L$ for the sparse code of each color channel. As a result,
 336 according to [41], the complexity of the QOMP algorithm is
 337 $\mathcal{O}(LM(\frac{14 \times m \times n}{3})^3)$, the complexity of the K-QSVD algorithm
 338 is $\mathcal{O}(LM(\frac{13 \times m \times n}{3})^3)$. The iteration of the proposed method in
 339 Algorithm 1 is T . In every iteration, we need to update \tilde{a}_{ij} with
 340 the QOMP algorithm. Overall, the complexity of our method as
 341 a whole is $\mathcal{O}(TLM(\frac{14 \times m \times n}{3})^3)$.

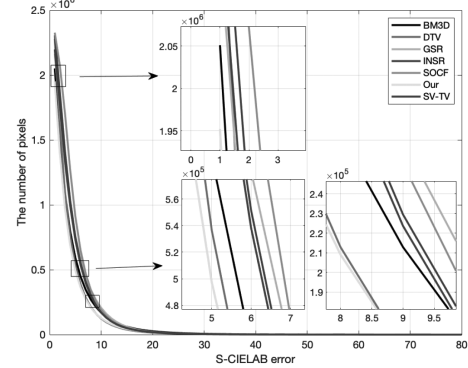
IV. EXPERIMENTAL RESULTS

342 To demonstrate the effectiveness of our quaternion-based dic-
 343 tionary learning and total variation method, we present the nu-
 344 matical and visual results in this section. We compare the pro-
 345 posed method with TV-based models (DTV [63], SV-TV [49]),
 346 DL-based methods (GSR [64], INSR [65]), sharpening opera-
 347 tor combined with framelet model (SOCF [66]), and the classic
 348 image processing method (BM3D [67]) for image restoration³.
 349

³The code of SV-TV [49] and SOCF [66] were provided by the corresponding authors; the code of DTV [63] was downloaded from [Online]. Available: <https://sites.google.com/site/thunsukeono/publications>; the code of GSR [64] was downloaded from [Online]. Available: <https://github.com/jianzhangcs/GSR>; the code of INSR [65] was downloaded from [Online]. Available: https://github.com/WanglifuCV/INSR_Deblur-SR; the code of BM3D [67] was downloaded from [Online]. Available: <https://webpages.tuni.fi/foi/GCF-BM3D/>.



(a) Results with ‘degraded=fspecial('gaussian',15,1)+noise’.



(b) Results with ‘degraded=fspecial('gaussian',15,1.5)+noise’.

Fig. 7. The average S-CIELAB errors between the ground-truth images and the restored results.

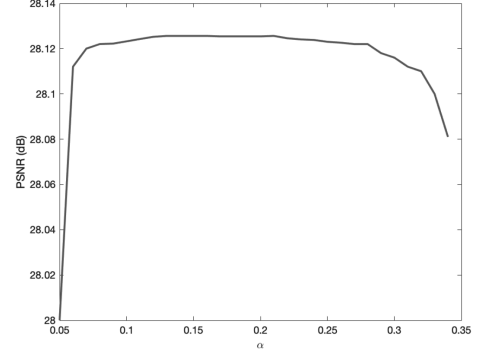
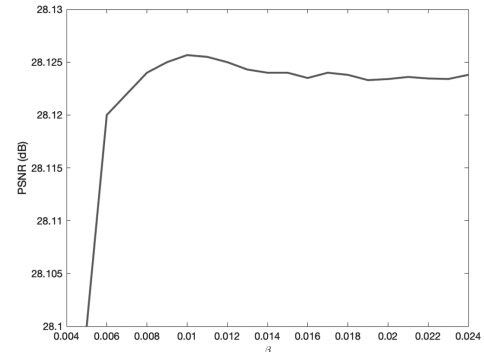
(a) PSNR values along with parameter α .(b) PSNR values along with parameter β .

Fig. 8. Parameters analysis. PSNR results of Img6 with ‘degraded=fspecial ('Gaussian',15,1)+noise’ by the proposed method.

TABLE II
PSNR AND SSIM VALUES OF COLOR IMAGE RESTORATION WITH GAUSSIAN KERNEL (15,1) AND NOISE LEVEL $\sigma = 12.75$

Images\Methods	Degraded	SOCF [66]	BM3D [67]	DTV [63]	SV-TV [49]	GSR [64]	INSR [65]	Ours
	PSNR SSIM	PSNR SSIM	PSNR SSIM	PSNR SSIM	PSNR SSIM	PSNR SSIM	PSNR SSIM	PSNR SSIM
Img1	25.70 0.8489	30.56 0.9556	32.76 0.9788	32.17 0.9480	32.24 0.9461	32.62 0.9662	31.93 0.9068	33.17 0.9826
Img2	27.37 0.8655	29.20 0.9583	35.02 0.9927	34.41 0.9519	34.39 0.9492	34.31 0.9802	34.99 0.9875	35.87 0.9929
Img3	25.54 0.7683	29.03 0.9084	30.19 0.9368	31.84 0.9492	31.23 0.9461	31.78 0.9325	31.82 0.9300	32.05 0.9357
Img4	23.54 0.6445	25.19 0.8094	25.63 0.8934	25.46 0.8996	26.12 0.8345	25.08 0.7963	25.36 0.7718	26.24 0.8996
Img5	22.96 0.7030	24.19 0.8282	24.01 0.8365	24.77 0.8790	24.87 0.8602	24.12 0.7932	24.86 0.8324	25.09 0.8872
Img6	24.38 0.7076	26.50 0.8094	26.95 0.8758	26.55 0.8519	26.62 0.8563	26.92 0.8914	27.23 0.9025	28.11 0.8932
Img7	25.05 0.6266	28.19 0.8439	28.28 0.8453	28.55 0.9100	28.78 0.9302	29.04 0.8619	29.11 0.8632	29.99 0.9193
Img8	23.81 0.8043	25.66 0.8883	25.83 0.8902	26.29 0.9243	26.19 0.9106	25.56 0.8696	25.52 0.8239	26.82 0.9329
Img9	24.71 0.7764	27.37 0.9050	27.96 0.9249	28.05 0.9363	28.33 0.8994	28.95 0.9324	28.97 0.9217	28.94 0.9370
Img10	24.57 0.7761	26.98 0.8857	27.78 0.8976	26.49 0.8820	26.67 0.9210	28.03 0.9025	28.18 0.9339	28.77 0.9551
Img11	24.52 0.6752	26.94 0.8329	27.60 0.8355	26.53 0.9111	26.84 0.9228	26.65 0.8767	26.77 0.7613	28.59 0.9030
Img12	23.87 0.7996	25.72 0.8767	26.15 0.8771	26.68 0.8914	26.64 0.8852	25.27 0.8582	25.12 0.8042	26.87 0.8915
Img13	24.22 0.6981	26.36 0.8547	26.64 0.8792	27.03 0.9044	27.00 0.8637	26.01 0.8292	25.81 0.8144	27.67 0.9052
Img14	24.14 0.6897	26.61 0.8766	27.64 0.9217	27.19 0.9200	27.60 0.8252	27.03 0.8950	27.12 0.8641	27.69 0.9192
Img15	24.93 0.5607	27.86 0.7826	28.48 0.8264	29.23 0.8576	29.22 0.8002	29.81 0.8195	29.73 0.8311	29.82 0.8537
Aver.	25.09 0.7295	27.92 0.8758	29.30 0.9036	29.10 0.9118	29.19 0.8997	29.51 0.9058	29.59 0.8892	30.29 0.9336

TABLE III
PSNR AND SSIM VALUES OF COLOR IMAGE RESTORATION WITH GAUSSIAN KERNEL (15,1.5) AND NOISE LEVEL $\sigma = 12.75$

Images\Methods	Degraded	SOCF [66]	BM3D [67]	DTV [63]	SV-TV [49]	GSR [64]	INSR [65]	Ours
	PSNR SSIM	PSNR SSIM	PSNR SSIM	PSNR SSIM	PSNR SSIM	PSNR SSIM	PSNR SSIM	PSNR SSIM
Img1	25.41 0.8445	30.59 0.9642	32.66 0.9806	31.94 0.9745	32.32 0.9725	32.64 0.9674	31.95 0.8809	32.72 0.9771
Img2	25.48 0.8824	29.93 0.9734	34.73 0.9918	33.56 0.9897	34.75 0.9897	33.88 0.9809	33.85 0.8983	34.95 0.9885
Img3	25.02 0.7428	28.87 0.9073	30.72 0.9150	29.08 0.8886	30.38 0.9145	31.00 0.9154	30.87 0.8538	31.18 0.9397
Img4	22.21 0.6002	23.78 0.8138	23.99 0.8562	24.56 0.8928	24.79 0.8559	23.87 0.7513	23.67 0.6482	24.91 0.8568
Img5	21.81 0.6549	23.09 0.8067	23.11 0.8077	23.04 0.8491	23.45 0.8428	22.56 0.7519	22.88 0.6960	23.53 0.8532
Img6	23.32 0.6621	25.60 0.8344	27.04 0.8774	26.63 0.8419	27.32 0.8812	27.31 0.8620	27.12 0.8893	27.33 0.8937
Img7	24.33 0.5859	27.20 0.8233	28.66 0.8530	28.35 0.8185	28.68 0.8348	28.80 0.8353	29.01 0.8141	29.20 0.8631
Img8	22.71 0.7632	24.59 0.8667	24.60 0.8602	25.04 0.8973	25.17 0.8983	23.77 0.8005	23.77 0.8005	25.65 0.9074
Img9	23.72 0.7449	26.17 0.8946	27.55 0.9192	27.54 0.9012	27.04 0.8773	29.81 0.8195	28.59 0.8632	29.91 0.9274
Img10	23.66 0.7433	26.03 0.8753	27.55 0.8989	27.35 0.8748	27.72 0.9025	28.00 0.8966	28.26 0.8605	28.27 0.8875
Img11	23.50 0.6214	25.64 0.7985	27.41 0.8335	26.17 0.7936	27.84 0.8426	27.88 0.8339	27.64 0.8604	27.49 0.8733
Img12	23.27 0.7763	25.32 0.8685	25.72 0.8695	25.28 0.8791	25.30 0.8794	23.61 0.7856	23.61 0.7856	26.03 0.8795
Img13	23.04 0.6549	25.11 0.8449	25.26 0.8505	24.94 0.8752	24.82 0.8708	24.16 0.7811	24.27 0.6947	25.58 0.8789
Img14	22.84 0.6603	24.77 0.8688	26.89 0.9189	28.60 0.8958	26.97 0.8522	30.03 0.8950	29.76 0.9023	30.34 0.8884
Img15	24.29 0.5248	27.29 0.7916	28.83 0.8348	28.58 0.8069	29.06 0.8198	29.81 0.8195	28.99 0.7946	29.83 0.8626
Aver.	23.64 0.6975	26.27 0.8621	27.30 0.8686	27.66 0.8944	27.71 0.8823	27.81 0.8464	27.62 0.8162	28.46 0.8983

350 The numerical quality of the restored images is measured by
351 S-CIELAB error⁴ [68], PSNR (peak signal-to-noise ratio), and
352 SSIM (structural similarity index measure) [69]. All test ex-
353 periments are conducted in MATLAB R2020a under macOS
354 Catalina 10.15.4 with a 1.40 GHz CPU and 8 GB memory.

355 A. Parameter Setting

356 The Dataset DIV2K⁵ [61] has a training set and a test set.
357 There are 800 images in the training set and 200 images in the
358 test set. We make use of images⁶ in Fig. 4 taken from the test set
359 of the DIV2K Dataset to test the proposed model for color image
360 restoration. We simulate the degraded images by convoluting
361 the original image in Fig. 4 with different Gaussian blur levels
362 (Matlab language *degraded=fspecial('Gaussian',15,1)*, and
363 *fspecial('Gaussian',15,1.5)*). Furthermore, we add the Gaussian
364 noise to model the unavoidable noise degradation in image

365 processing. For Gaussian blur (15,1), we set $\lambda = 0.5$, $\eta = 0.5$,
366 $\alpha = 0.22$, $\beta = 0.01$ for our method. For Gaussian blur (15,1.5),
367 we set $\eta = 0.4$. The parameters of other methods are the default
368 values or the corresponding values described in their articles
369 and codes. We break the ADMM iteration when the relative
370 error of the successive iterates is less than or equal to 10^{-5} for
371 all the testing methods.

372 B. Our Strategy

373 With the fixed dictionary, by updating the subproblems under
374 the framework of the ADMM algorithm, the final restoration re-
375 sult is obtained. The convergence of Img6 is given in Fig. 5 to
376 illustrate the effectiveness of the proposed model. As the itera-
377 tion goes, the PSNR (dB) value is going to stability. Due to the
378 proposed model combines different regularizers for color image
379 restoration, we display the analysis of the balance parameters η
380 and λ in a small interval in Fig. 6. In the test, we choose differ-
381 ent η and λ by trial and error to produce the best possible result.
382 The PSNR and SSIM curves become quite flat as the parameter η
383 from 0.3 to 0.8 along the η axis, which implies choosing $\eta = 0.5$
384 ensures the best result of the test Img6. We choose the parameter
385 η in the interval [0.3,0.8] for other test images. The curve along

⁴S-CIELAB code is in [Online]. Available: <http://scarlet.stanford.edu/brian/scielab/scielab.html>.

⁵[Online]. Available: <https://data.vision.ee.ethz.ch/cvl/DIV2K/>.

⁶Image size: Img1, 2, 3, 7, 10, 11, 12, 13 with 2040 × 1356; Img 4, 5 with 2040 × 1536; Img 6 with 2040 × 1200; Img 14 with 2040 × 1152; Img 8 with 2040 × 1284; Img 9 with 1356 × 2040; Img 15 with 2040 × 2040.

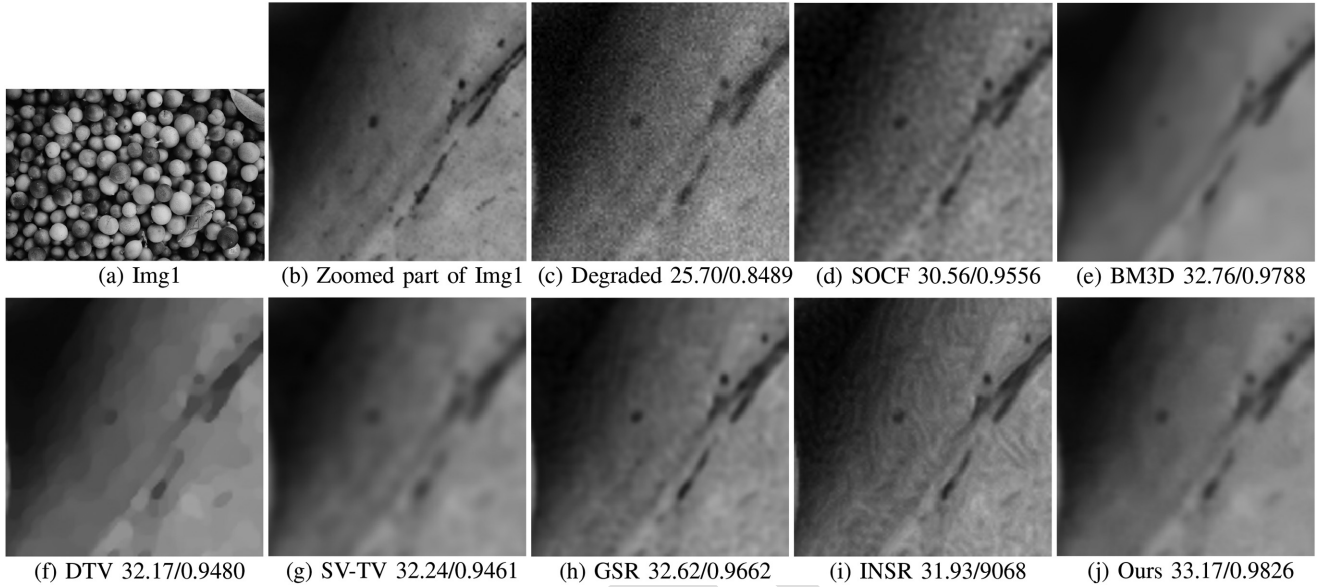


Fig. 9. Color image restoration results on Img1. (a) Original image; (b) The zoomed part of Img1; (c) Gaussian blur (15,1) and Gaussian noise level $\sigma = 12.75$; The zoomed part of restored image reconstructed by: (d) SOCF [66], (e) BM3D [67], (f) DTV [63], (g) SV-TV [49], (h) GSR [64], (i) INSR [65], and (j) Ours.

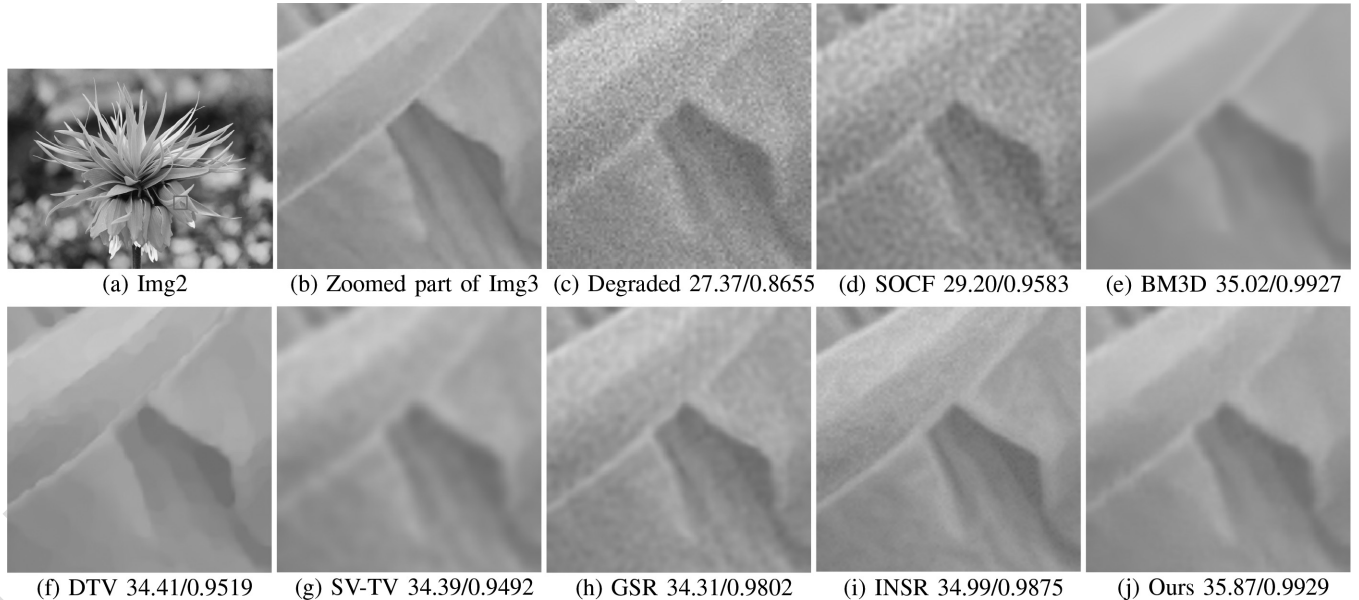


Fig. 10. Color image restoration results on Img2. (a) Original image; (b) The zoomed part of Img2; (c) Gaussian blur (15,1) and Gaussian noise level $\sigma = 12.75$; The zoomed part of restored image reconstructed by: (d) SOCF [66], (e) BM3D [67], (f) DTV [63], (g) SV-TV [49], (h) GSR [64], (i) INSR [65], and (j) Ours.

386 λ almost has a wider peak in $(0.1, 0.9]$, which gives more choices
 387 of λ . Here, we find a small interval $(0.1, 0.9]$, such that the results
 388 are robust to the parameter λ . The analysis of parameters α and
 389 β are also conducted in Fig. 8. We set $\alpha \in [0.05, 0.34]$ with step
 390 size 0.01 and $\beta \in [0.005, 0.015]$ with step size 0.001. How to
 391 select the related parameters automatically is an open question.
 392 We leave this as future works.

393 C. Experimental Results

394 Since the CIELAB system [70] is an important international
 395 standard for measuring color reproduction errors, we test the
 396 results with the S-CIELAB error indicator [68]. The S-CIELAB

397 error evaluates the error between a pair of images. For 15 images
 398 in Fig. 4, we find that when the S-CIELAB error becomes 70,
 399 all the error pixels number of restored images by the methods
 400 we tested equate to zero. We set the error from 0 to 80 so that
 401 the S-CIELAB indicator can calculate the error number of these
 402 image pairs. Here error = 0 means the two images are the same.
 403 As the S-CIELAB error goes, the number of error pixels decreases.
 404 We plot the average S-CIELAB errors of all 15 images in Fig. 7,
 405 which shows the restored image of our method has the least total
 406 error pixel number. It becomes clear that the proposed method
 407 outperforms other testing methods in terms of the S-CIELAB
 408 color metric when the S-CIELAB error less than 10 units.

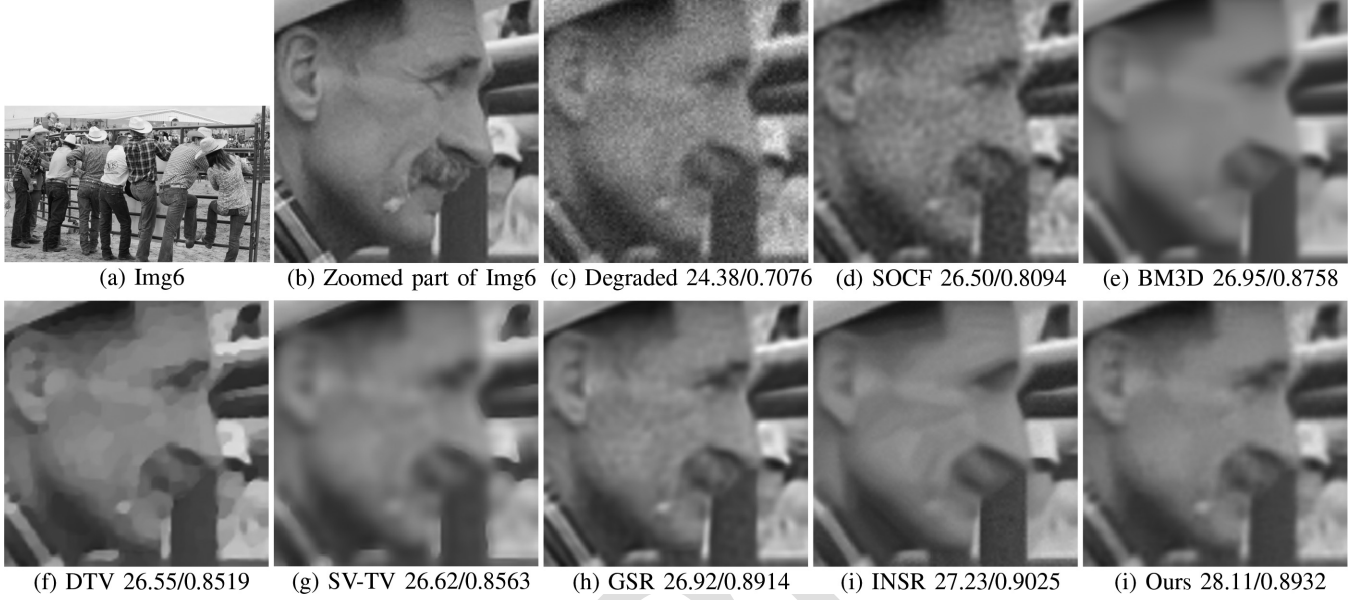


Fig. 11. Color image restoration results on Img6. (a) Original image; (b) The zoomed part of Img6; (c) Gaussian blur (15,1) and Gaussian noise level $\sigma = 12.75$; The zoomed part of restored image reconstructed by: (d) SOCF [66], (e) BM3D [67], (f) DTV [63], (g) SV-TV [49], (h) GSR [64], (i) INSR [65], and (j) Ours.

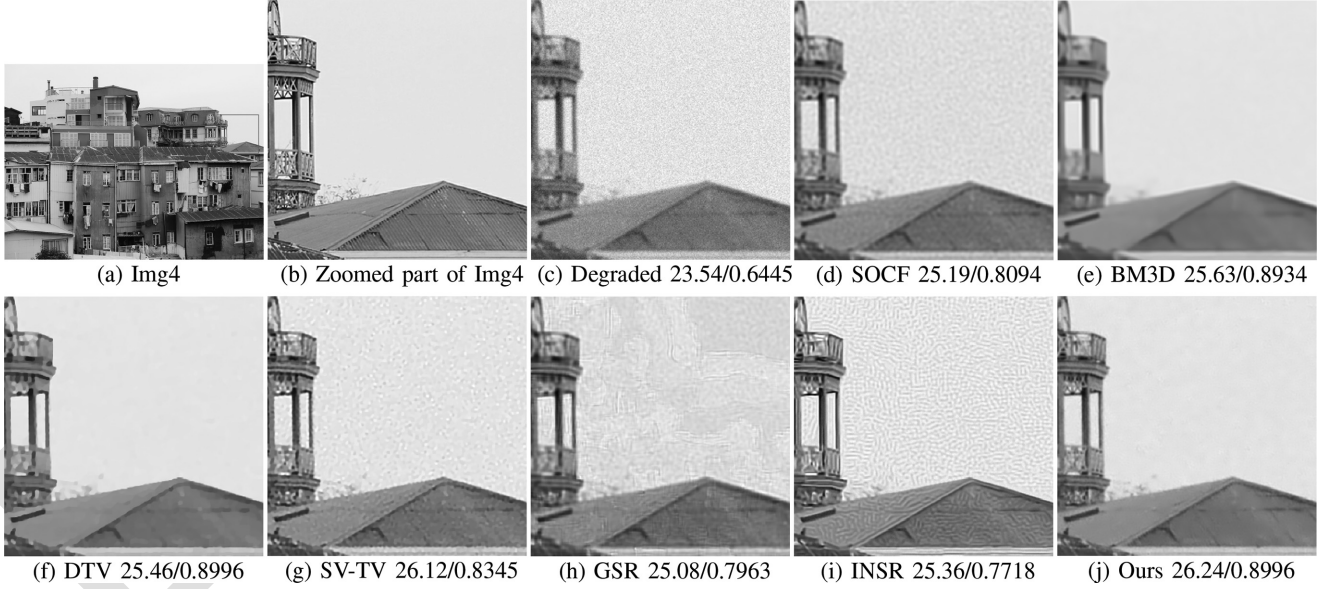


Fig. 12. Color image restoration results on Img4. (a) Original image; (b) The zoomed part of Img4; (c) Gaussian blur (15,1.5) and Gaussian noise level $\sigma = 12.75$; The zoomed part of restored image reconstructed by: (d) SOCF [66], (e) BM3D [67], (f) DTV [63], (g) SV-TV [49], (h) GSR [64], (i) INSR [65], and (j) Ours.

409 The numerical results of the SSIM and PSNR values are
410 present in Table II and Table III. The highest PSNR and SSIM
411 values are highlighted in bold and the second-highest ones are
412 underlined. The average PSNR and SSIM values of all compared
413 methods are also computed. We find that most of our results out-
414 perform other competing methods' results in terms of the PSNR
415 and SSIM values, which further verifies the advantages of our
416 method. For visual quality, we display the recovered results of
417 our experiments in Fig. 9, Fig. 10, and Fig. 11 for the blur ker-
418 nel of standard deviation 1 and white Gaussian noise of standard

419 deviation $\sigma = 12.75$. Fig. 12, Fig. 13, and Fig. 14 show the blur
420 kernel of standard deviation 1.5 and white Gaussian noise of
421 standard deviation $\sigma = 12.75$. The quality of the restored images
422 can be evaluated visually besides the values. From the visual re-
423 sults, we know that the restored images of the SOCF method still
424 have some color spots. The DTV method tends to smooth the
425 textures in the restored images. The SV-TV method is good at
426 handling image noise, while the results show that this method is
427 not very expert in blur removal. For the classical BM3D method,
428 the results seem to oversmooth. As for the dictionary learning

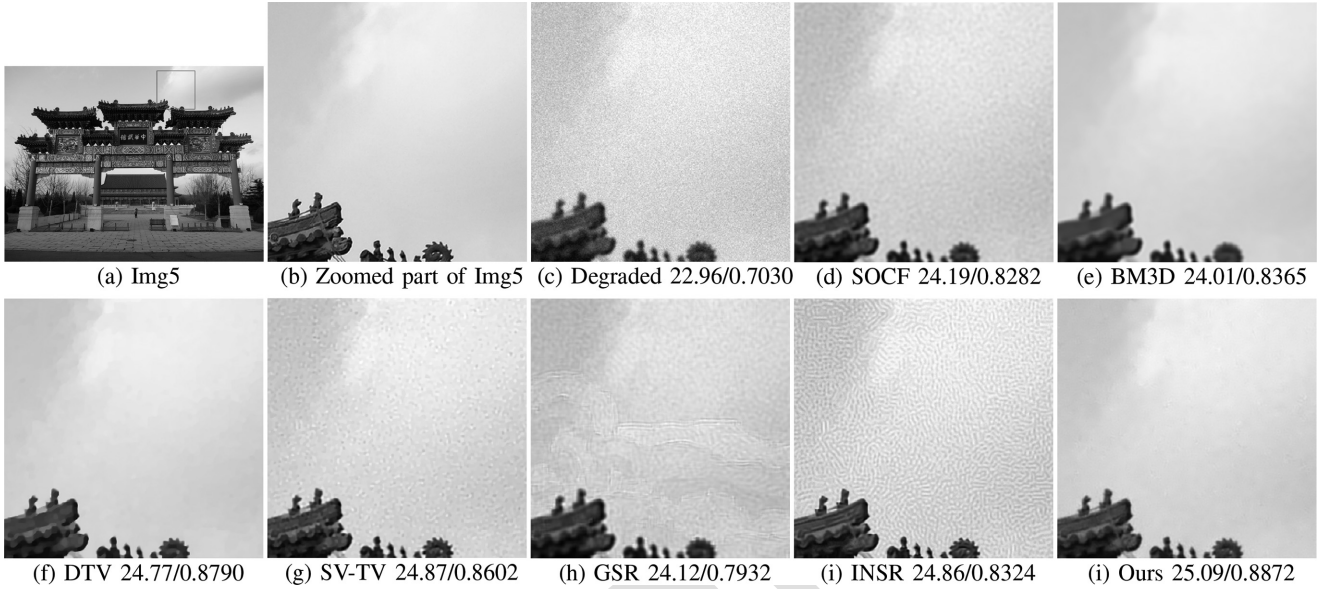


Fig. 13. Color image restoration results on Img5. (a) Original image; (b) The zoomed part of Img5; (c) Gaussian blur (15,1.5) and Gaussian noise level $\sigma = 12.75$; The zoomed part of restored image reconstructed by: (d) SOCF [66], (e) BM3D [67], (f) DTV [63], (g) SV-TV [49], (h) GSR [64], (i) INSR [65], and (j) Ours.

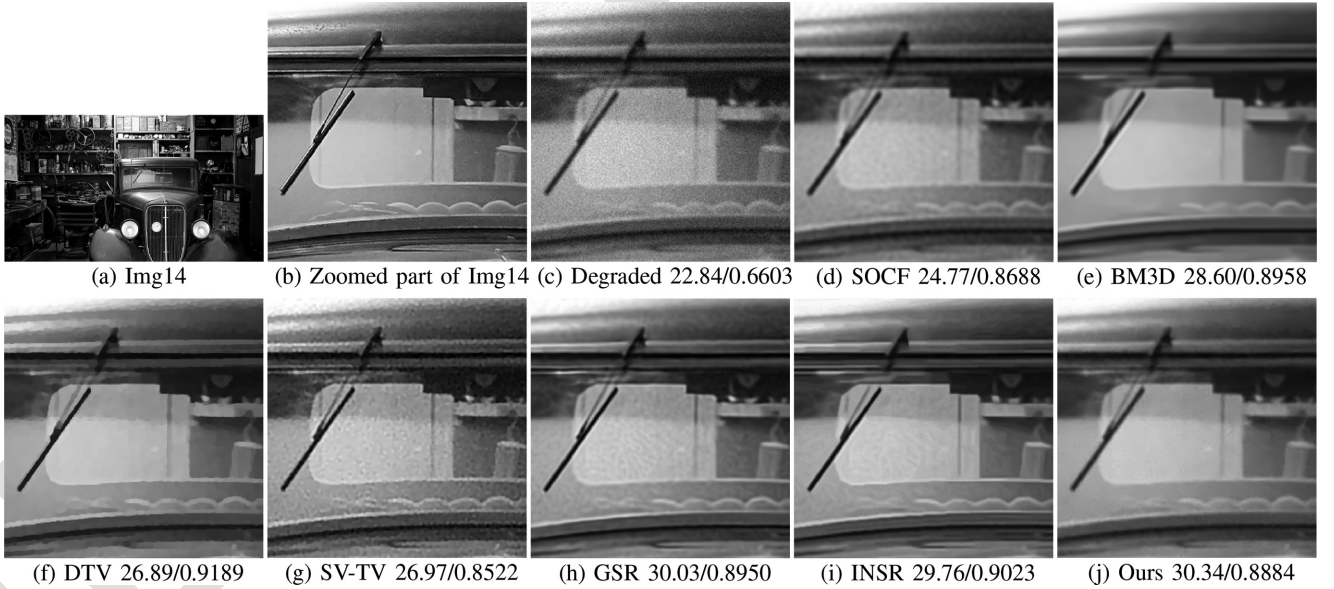


Fig. 14. Color image restoration results on Img14. (a) Original image; (b) The zoomed part of Img14; (c) Gaussian blur (15,1.5) and Gaussian noise level $\sigma = 12.75$; The zoomed part of restored image reconstructed by: (d) SOCF [66], (e) BM3D [67], (f) DTV [63], (g) SV-TV [49], (h) GSR [64], (i) INSR [65], and (j) Ours.

429 method INSR and GSR, the artifacts can be found clearly. Our
430 method can better restore the degraded images and remove the
431 artifacts generated by the patch-based method.

432 V. CONCLUSION

433 In this paper, we propose an effective method that combines
434 pure quaternion dictionary learning and SV-TV regularizers for
435 color image recovery. For color image processing, we represent
436 the color image with the pure quaternion matrix. In this case,
437 the inner relationship of the color image can be well preserved.

438 The patch-based dictionary learning method always generates
439 some unsatisfied artifacts. We apply SV-TV to overcome these
440 artifacts. Compared with some state-of-the-art image restoration
441 methods, our model can preserve more texture details and avoid
442 the generation of artifacts. In summary, the method we proposed
443 achieves great success in numerical and visual results.

444 Since the parameters of different test images are quite differ-
445 ent, it may not be good enough to tune parameters manually.
446 Hence, how to determine the parameters automatically will be
447 our future work.

448

449

450

451

452

453

454

455

456

457

458

459

460

461

462

463

464

465

466

467

468

469

470

471

472

473

474

475

476

477

478

479

480

481

482

483

484

485

486

487

488

489

490

491

492

493

494

495

496

497

498

499

500

501

502

503

504

505

506

507

508

509

510

511

512

513

514

515

516

517

518

519

520

521

522

523

524

525

526

527

528

529

530

531

532

533

534

535

536

537

538

539

540

541

542

543

544

545

546

547

548

549

550

551

552

553

554

555

556

557

558

559

560

561

562

563

564

565

566

567

568

569

570

571

572

573

574

575

576

577

578

579

580

581

582

583

584

585

586

587

588

589

590

591

592

593

594

595

596

597

598

599

600

601

602

603

604

605

606

607

608

609

610

611

612

613

614

615

616

617

618

619

620

621

622

623

624

625

626

627

628

629

630

631

632

633

634

635

636

637

638

639

640

641

642

643

644

645

646

647

648

649

650

651

652

653

654

655

656

657

658

659

660

661

662

663

664

665

666

667

668

669

670

671

672

673

674

675

676

677

678

679

680

681

682

683

684

685

686

687

688

689

690

691

692

693

694

695

696

697

698

699

700

701

702

703

704

705

706

707

708

709

710

711

712

713

714

715

716

717

718

719

720

721

722

723

724

725

726

727

728

729

730

731

732

733

734

735

736

737

738

739

740

741

742

743

744

745

746

747

748

749

750

751

752

753

754

755

756

757

758

759

760

761

762

763

764

765

766

767

768

769

770

771

772

773

774

775

776

777

778

779

780

781

782

783

784

785

786

787

788

789

790

791

792

793

794

795

796

797

798

799

800

801

802

803

804

805

806

807

808

809

810

811

812

813

814

815

816

817

818

819

820

821

822

823

824

825

826

827

828

829

830

831

832

833

834

835

836

837

838

839

- [52] S. W. Zamir *et al.*, "Learning enriched features for real image restoration and enhancement," in *Proc. Eur. Conf. Comput. Vision (ECCV)*, 2020, pp. 492–511.
- [53] M. Zach and E. Kobler, "Real-world video restoration using Noise2Noise," in *Proc. Joint Austrian Comput. Vis. Robot. Workshop. Verlag der Technischen Universität Graz*, 2020, pp. 145–150.
- [54] Y. Chen, Z. Jia, Y. Peng, and Y. Peng, "Robust dual-color watermarking based on quaternion singular value decomposition," *IEEE Access*, vol. 8, pp. 30 628–30 642, 2020.
- [55] W. R. Hamilton, *Elements of Quaternions*. London: Longmans, Green, & Company, 1866.
- [56] Z. Jin, F. Li, and M. K. Ng, "A variational approach for image decolorization by variance maximization," *SIAM J. Imag. Sci.*, vol. 7, no. 2, pp. 944–968, 2014.
- [57] D. Gabay and B. Mercier, "A dual algorithm for the solution of nonlinear variational problems via finite element approximations," *Comput. Math. Appl.*, vol. 2, pp. 17–40, 1976.
- [58] L. Chen, X. Li, D. Sun, and K.-C. Toh, "On the equivalence of inexact proximal ALM and ADMM for a class of convex composite programming," *Math. Program.*, vol. 185, pp. 111–161, 2021.
- [59] L. Chen, D. Sun, and K.-C. Toh, "A note on the convergence of ADMM for linearly constrained convex optimization problems," *Comput. Optim. Appl.*, vol. 66, no. 2, pp. 327–343, 2017.
- [60] S. Boyd, N. Parikh, E. Chu, B. Peleato, and J. Eckstein, "Distributed optimization and statistical learning via the alternating direction method of multipliers," *Found. Trends Mach. Learn.*, vol. 3, no. 1, pp. 1–122, 2011.
- [61] A. Ignatov *et al.*, "PIRM challenge on perceptual image enhancement on smartphones: Report," in *Proc. Eur. Conf. Comput. Vis. Workshops*, 2019, pp. 1–18.
- [62] Y. Wang, J. Yang, W. Yin, and Y. Zhang, "A new alternating minimization algorithm for total variation image reconstruction," *SIAM J. Imag. Sci.*, vol. 1, pp. 248–272, 2008.
- [63] S. Ono and I. Yamada, "Decorrelated vectorial total variation," *Proc. IEEE Conf. Comput. Vis. Pattern Recognit.*, 2014, pp. 4090–4097.
- [64] J. Zhang, D. Zhao, and W. Gao, "Group-based sparse representation for image restoration," *IEEE Trans. Image Process.*, vol. 23, no. 8, pp. 3336–3351, Aug. 2014.
- [65] N. Wang, W. Shi, C. Fan, and L. Lou, "An improved nonlocal sparse regularization-based image deblurring via novel similarity criteria," *Int. J. Adv. Robot. Syst.*, vol. 15, pp. 1–18, 2018.
- [66] J.-J. Liu, Y. Lou, G. Ni, and T. Zeng, "An image sharpening operator combined with framelet for image deblurring," *Inverse Problems*, vol. 36, no. 045015, pp. 1–27, 2020.
- [67] A. Danielyan, V. Katkovnik, and K. O. Egiazarian, "BM3D frames and variational image deblurring," *IEEE Trans. Image Process.*, vol. 21, no. 4, pp. 1715–1728, Apr. 2012.
- [68] X. Zhang and B. Wandell, "A spatial extension of CIELAB for digital color-image reproduction," *J. Soc. Inf. Display*, vol. 5, pp. 61–63, 1997.
- [69] Z. Wang, A. Bovik, H. R. Sheikh, and E. P. Simoncelli, "Image quality assessment: From error visibility to structural similarity," *IEEE Trans. Image Process.*, vol. 13, no. 4, pp. 600–612, Apr. 2004.
- [70] A. Robertson *et al.*, "CIE recommendations on uniform color spaces, color-difference equations, and metric color terms," *Color Res. Appl.*, vol. 2, no. 1, pp. 5–6, 1977.

Chaoyan Huang received the B.S. degree with the College of Mathematics and Computer Science, Anqing Normal University, Anqing, China, in 2019. She is currently working toward the M.S. degree with the School of Science, Nanjing University of Posts and Telecommunications, Nanjing, China. Her research interests include image processing, inverse problems, and machine learning.



Michael K. Ng received the B.Sc. and M.Phil. degrees from the University of Hong Kong, Hong Kong, in 1990 and 1992, respectively, and the Ph.D. degree from the Chinese University of Hong Kong, Hong Kong, in 1995. He is currently a Chair Professor with the Department of Mathematics, University of Hong Kong. His research interests include bioinformatics, image processing, scientific computing, and data mining.



Tingting Wu received the B.S. and Ph.D. degrees in mathematics from Hunan University, Changsha, China, in 2006 and 2011, respectively. From 2015 to 2018, she was a Postdoctoral Researcher with the School of Mathematical Sciences, Nanjing Normal University, Nanjing, China. From 2016 to 2017, she was a Research Fellow with Nanyang Technological University, Singapore. She is currently an Associate Professor with the School of Science, Nanjing University of Posts and Telecommunications, Nanjing, China. Her research interests include variational methods for image processing and computer vision, optimization methods and their applications in sparse recovery, and regularized inverse problems.



methods for image processing and computer vision, optimization methods and their applications in sparse recovery, and regularized inverse problems.

Tieyong Zeng received the B.S. degree from Peking University, Beijing, China, in 2000, the M.S. degree from École Polytechnique, Palaiseau, France, in 2004, and the Ph.D. degree from the University of Paris XIII, Paris, France, in 2007. He was a Postdoctoral Researcher with ENS de Cachan, Cachan, France, since 2007 to 2008, and an Assistant/Associate Professor with Hong Kong Baptist University, Hong Kong, since 2008 to 2018. He is currently a Professor with the Department of Mathematics, The Chinese University of Hong Kong, Hong Kong. His research interests include image processing, machine learning, and scientific computing.

